[AMERICAN JOURNAL OF SCIENCE, VOL. 296, JANUARY, 1996, P. 23–57]

MESOSCOPIC STRUCTURE, STRAIN, AND VOLUME LOSS IN FOLDED COVER STRATA, VALLEY AND RIDGE PROVINCE, MARYLAND

MICHELLE MARKLEY* and STEVEN WOJTAL
Department of Geology,
Oberlin College,
Oberlin, Ohio 44074

ABSTRACT. In ~200 m wavelength folds in Silurian strata exposed in the western part of the Valley and Ridge Province in Maryland, two morphologically distinct cleavages contribute to total shortening. Large solution seams that may cross several beds at nearly right angles define an early, pre-folding, cleavage; this early cleavage accommodated at least 10 percent layer-parallel shortening along a northwest azimuth with nearly 10 percent volume loss. Finite-amplitude folding accommodated later layer shortening along a nearly west-northwest azimuth; a second cleavage formed during fold growth in concert with calcite-filled veins, bedding-parallel slip surfaces, and bedding-parallel shear zones which we call cleavage-slip zones. Rotation of beds during fold amplification yields 18 percent shortening in the strata we examine in detail, and the later cleavage and cleavage-slip zones together account for 10 to 15 percent of sub-horizontal shortening and 10 to 15 percent volume loss. Total shortening in these strata must be at least 25 percent (early cleavage shortening plus profile shortening due to folding), and it may be as much as 40 percent when shortening due to the later cleavage is considered. This magnitude of layer-parallel shortening exceeds previous estimates for shortening in Silurian to Devonian strata in this region. Furthermore, different azimuths for shortening have not been suggested before for this portion of the belt.

Measurements of strain and quantitative analysis of mesoscopic structures across a symmetrical anticline among these folds suggest fold growth by a simultaneous combination of flexural flow and flexural slip. Flexural slip and flexural flow made different net contributions to fold growth on the two limbs of the anticline. The number of active bedding-parallel slip zones apparently increased on both limbs as the fold grew, causing changes in the bulk behavior of the strata involved in folding. Our study of strain and mesoscopic structures in this fold suggests that buckling was the dominant mechanism of folding and that differences in evolving mesoscopic structures had consequences for the subsequent development of folds.

INTRODUCTION

The central Appalachian Valley and Ridge Province exhibits a three-tiered structural architecture with (1) late Proterozoic crystalline and sedimentary rocks and early Paleozoic volcanics and clastics in basement, (2) detached and imbricated Cambro-Ordovician carbonates, and (3) predominantly siliciclastic, mainly folded post-Upper Ordovician strata (Gwinn, 1964, 1970; Perry, 1978) (fig. 1). Thrusting is the primary

* Present address: Department of Geology and Geophysics, University of Minnesota, Minneapolis, Minnesota 55455.

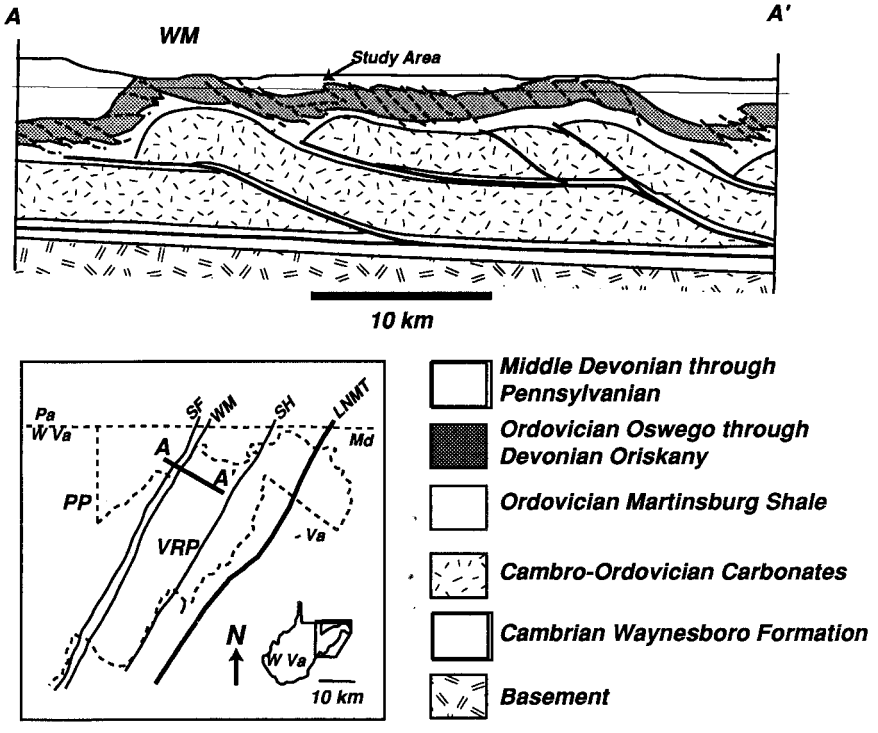

Fig. 1. Regional cross section and location map, from Schumaker and Wilson (1992). Thick line AA' on location map denotes the line of section. The arrow on the cross section indicates the location of the study area. PP = Plateau Province, VRP = Valley and Ridge Province, GVP = Great Valley Province, SF = Alleghenian structural front, WM = Wills Mountain anticlinorium, LNMT = Little North Mountain thrust. SH = Sideling Hill syncline.

shortening mechanism in the lower Paleozoic carbonates, and the geometry of the thrusts that cut these strata dictates the megascopic structure of the post-Upper Ordovician strata near the surface (Schumaker and others, 1985; Wilson and Schumaker, 1992). Strata in regional synclinoria are detached but lie essentially at their regional dip (Perry and de Witt, 1977; Perry, 1978). Regional anticlinoria are either passive kinks (Faill, 1973) or fault-related folds (Suppe, 1983, 1985; Jamison, 1987) above duplicated Cambro-Ordovician strata. Following the terminology in Geiser (1988a,b), we call the mainly folded Upper Ordovician and younger strata above the thrust-faulted carbonates *cover strata.* In the cover strata, folding at shorter wavelengths, outcrop-scale faulting, and pervasive solution transfer contribute to stratal shortening (Mitra, 1987; Geiser, 1988a; Dunne, 1988; Meyer and Dunne, 1990). A thick package of shales, the Ordovician Martinsburg Formation, separates the cover strata from the imbricated carbonates, however, and this unit is too

poorly exposed to constrain hypotheses on how shortening in the thrust-faulted Cambro-Ordovician carbonates links with that in the post-Ordovician cover strata. One aim of our examination near the Pennsylvania-Maryland state line was to determine whether and how thrust-related shearing affected shortening in cover strata, particularly during the formation of ubiquitous ~200 m wavelength folds.

Balanced cross sections across the central Appalachian Valley and Ridge Province yield large differences in restored bed lengths for the imbricated carbonates and the cover strata (Geiser, 1988a,b). Extensive layer-parallel shortening by solution transfer preceded finite-amplitude folding in cover strata (Geiser, 1974; Perry, 1978), which may account for some of the missing length of cover strata in restorations (Engelder and Geiser, 1979; Geiser, 1988a,b). A second aim of our study was to ascertain the extent to which volume loss by solution transfer prior to folding or faulting contributed to stratal shortening in the cover sequence.

Siluro-Devonian cover strata in synclinoria in western Maryland and West Virginia exhibit relatively regular trains of upright to overturned, open to tight folds with angular to rounded profiles and wavelengths of 150 to 250 m (de Witt and Colton, 1964; Geiser, 1974; Perry and de Witt, 1977) (fig. 2). Fold hinges trend generally north-northeast and plunge gently to the north and south away from minor structural culminations. Slickensides on bedding indicate that flexural slip contributed to the formation of these folds. Removal of material across solution seams inclined to bedding also accommodated flexural flow. Solution transfer accommodated significant layer-parallel shortening and volume loss. The third aim of our study was to use deformation microstructures and finite strain data in cover strata to infer the mechanisms by which folds developed.

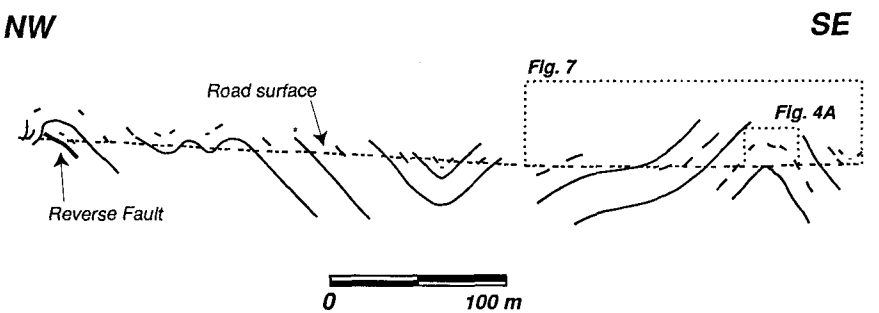

Fig. 2. Fold profile (drawn on a plane whose normal is 028, 07) showing pitch of bedding in folds in the Tonoloway Limestone exposed near the crest of Martin Mountain (on the northwest limb of the Tussey Mountain anticlinorium) in western Maryland. The subhorizontal dashed line indicates the projected position of the road along which we collected most of our data. Bedding traces taken from field measurements and photographs of exposures. Locations taken from a plane-table map of the exposure. The dashed boxes at right denote the areas shown in figures 4A and 7. No vertical exaggeration.

MESOSCOPIC AND MICROSCOPIC STRUCTURES

We mapped deformation structures and microstructures in upright, sinusoidal folds in Silurian limestones and dolostones of the Tonoloway Limestone. The data we present here are from strata exposed in a road cut on route U.S. 40, near the crest of Martin Mountain (de Witt and Colton, 1964; Perry and de Witt, 1977) (fig. 1); we focus on the deformation elements in a very well exposed anticline at the eastern end of these exposures (figs. 2 and 4A). The folds are approximately cylindrical, and poles to primary bedding fall along a well defined great-circle girdle whose normal plunges gently to the north-northeast (fig. 3A).

Movement horizons.—Some beds were welded together by bedding-parallel diagenetic stylolites, but smooth bedding surfaces often have slickensides (fig. 4B and C). The sense of slip on slickensided bedding surfaces, inferred from mineral-fiber geometry, offset veins, and deflected solution seams, is symmetrical about the anticline hinge. No slickensides were observed on the beds in fold hinges, indicating that the folds had pinned hinges. Slip occurred on some individual, laterally-extensive, smooth bedding planes. In other cases, slip occurred on subparallel surfaces connected by oblique ramps that step from one bed to another. These individual movement horizons (Tanner, 1989) are confined to thin, well-defined stratigraphic sequences on each limb. Bedding slip surfaces or movement horizons sometimes occur at equivalent stratigraphic positions on opposing limbs. In many cases, however, bedding slip surfaces or movement horizons occur at different stratigraphic positions on opposing limbs. The mean bed-normal spacing between movement horizons is slightly but statistically different on the two limbs (figs. 5 and 6).

Packets of well-aligned, untwinned calcite fibers, one to 10 mm thick, compose most bedding slickensides; they are slickenfibers (Tanner, 1989). Blocky, randomly-oriented calcite crystals replace fibers in the central portions of some fiber packets. Z. Zadins (personal communication) argues that such a microstructure forms by outward migration of the active slip surface within the packet of fibers that compose a slickenside. Other slickensides are ridges-and-grooves (Means, 1987) on the bounding surfaces of interlayered selvage and secondary calcite. We infer that slickenfibers and ridge-and-groove slickensides are related to a penetrative cleavage, and we outline below a hypothesis for their formation. Kinematic rotation axes (Price, 1967) or slip normals for calcite-fiber slickensides and ridge-and-groove slickensides together define a point maximum coincident with the pole of the bedding circle (fig. 3B). We infer, then, that bedding slickensides formed during folding and that this anticline is locally nearly cylindrical (Dubey, 1982).

Calcite-fiber slickensides have an average thickness of 5 mm and a mean spacing of 0.70 m on the west limb and 0.84 m on the east limb of the anticline (actual spacing varies from 0.04-3 m). Thus, they account for just less than 1 percent elongation normal to bedding and just less than 1

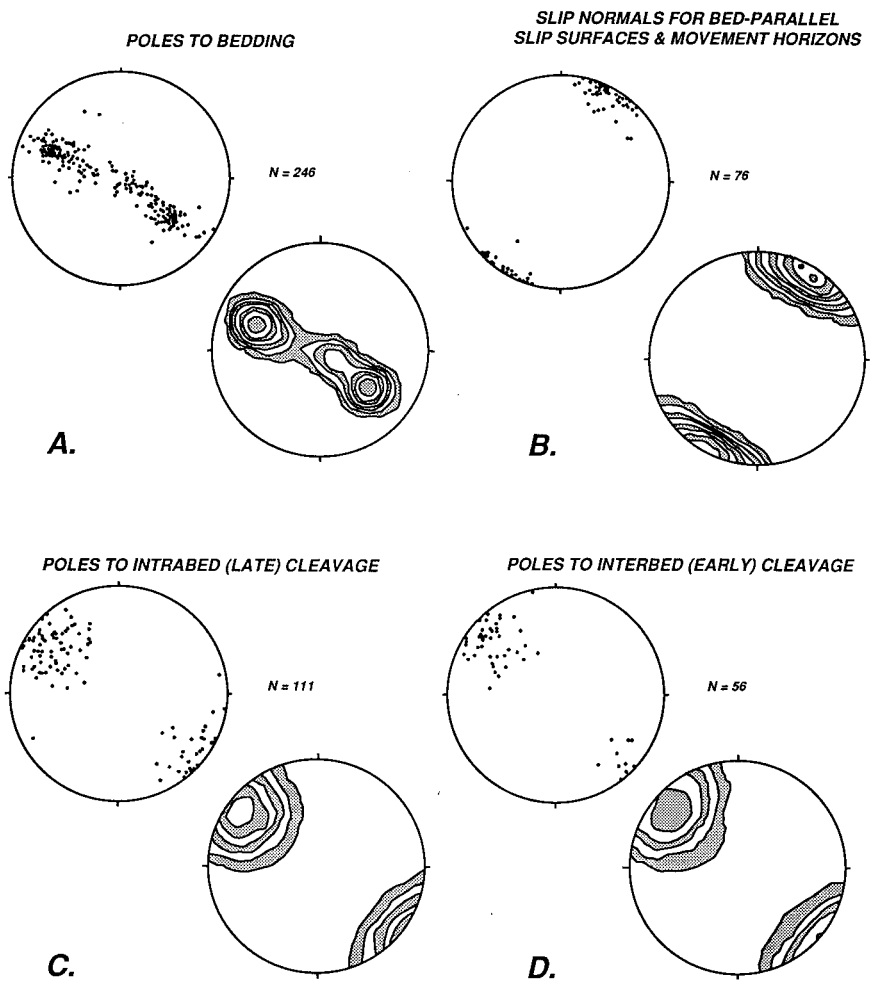

Fig. 3. Paired stereonets (scatter plot and contoured diagram) give the attitudes of mesoscopic structural features in folds in the Silurian Tonoloway Limestone. N = sample size; contours in multiples of 3σ, three times the calculated standard deviation of a random distribution of points equal in number to the sample size (Kamb, 1959). (A) Poles to bedding. Bedding poles define a great circle whose normal is 028, 07. (B) Slip normals or kinematic rotation axes for bed-parallel movement zones. The point maximum for slip normals is 029, 07. (C) Poles to intrabed (late) cleavage. The pole to the best fit great circle through these points is 037, 04. (D) Poles to interbed (early) cleavage. The pole to the best fit great circle through these points is 043, 05.

percent total volume increase. Compared to the stratal thinning and volume loss associated with the formation of the two morphologically and geometrically distinctive solution cleavages that we recognize in these folds and discuss below, this volume increase is negligible.

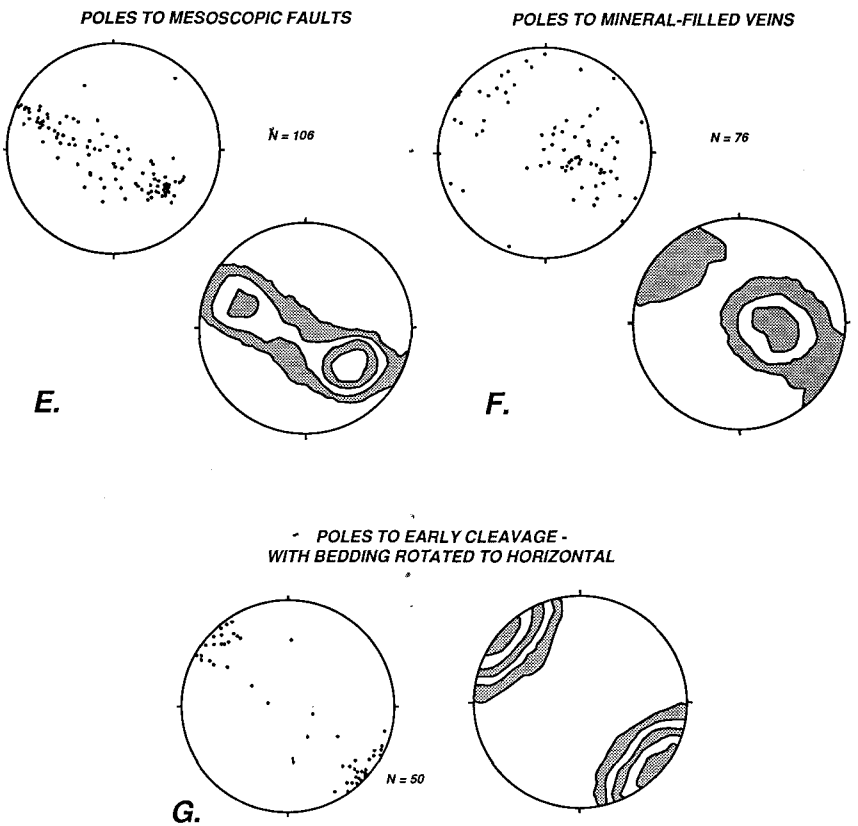

Fig. 3(E) Poles to mesoscopic fault surfaces. Poles to faults define a great circle whose normal is 029,12. (F) Poles to mineral-filled veins. The pole to the diffuse great circle girdle defined by these points is 214, 30. (G) Rotated poles to interbed cleavage, determined by rigidly rotating cleavage pole through the same angle needed to bring bedding to horizontal. The bearing of the point maximum for rotated poles to cleavage is 308.

Interbed cleavage.—Widely spaced solution seams at high angles to bedding characterize the first cleavage. Because the individual seams defining this cleavage typically extend from one bed into neighboring beds (fig. 4B, C, and D), we call this cleavage *interbed cleavage.* In the grainstones (terminology from Meyer and Dunne, 1990) where they are most easily recognized, interbed cleavage seams have wavy to sutured morphologies (Engelder and Marshak, 1985), thick selvage accumulations, and well-developed steps nearly normal to the seams. Interbed cleavage seams typically are within 5° of normal to bedding in grainstones (fig. 4B, C, and D); this cleavage fans convergently (Ramsay 1967, p. 405) about the anticline. Where recognized in mudstones (terminology from Meyer and Dunne, 1990), interbed cleavage seams exhibit wavy to

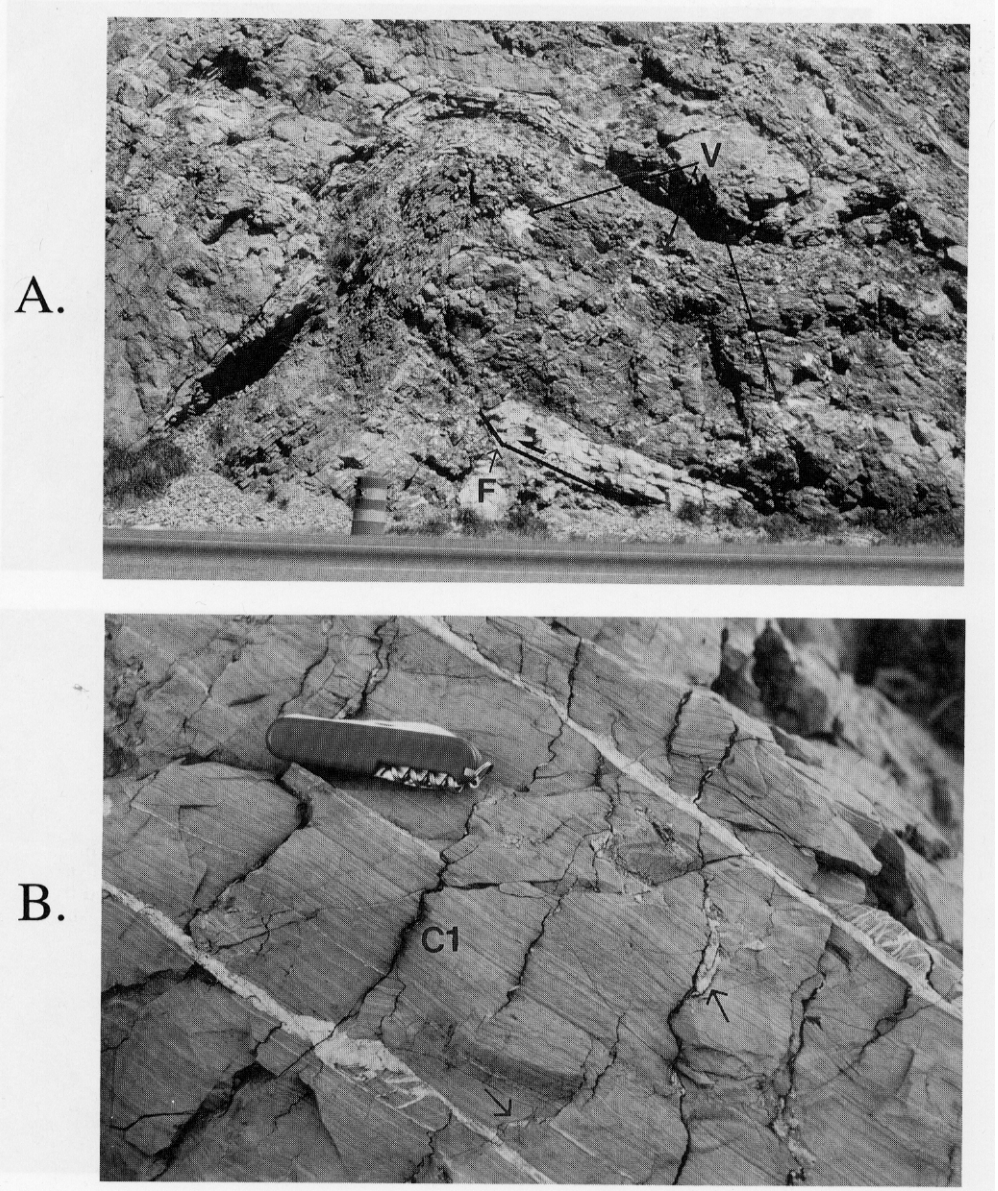

Fig. 4. Photographs of mesoscopic structures in the anticline examined in detail. (A) Hinge region of the anticline, showing dolomite bed cut by limb thrust (F) and extensive vein growth (V). (B) Solution seams of the interbed cleavage (C1) cut by bedding-parallel slip surfaces; note that secondary calcite also fills openings along some interbed cleavage seams (arrows).

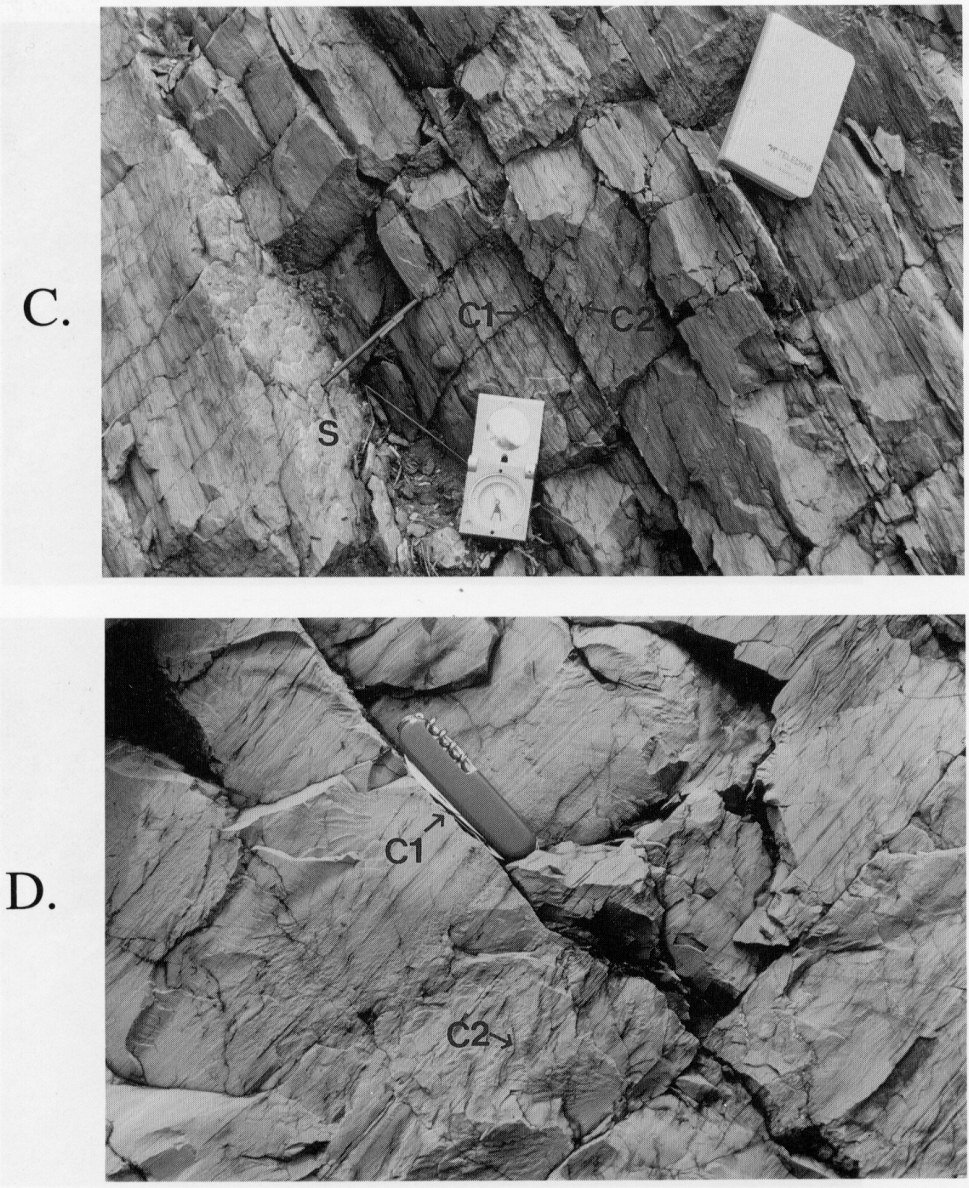

Fig. 4(C) Calcareous grainstones with distinct interbed cleavage seams oriented nearly normal to bedding (C1) and intrabed cleavage seams inclined to bedding (C2). Slip surface (S) with calcite-fiber slickensides cuts up section through bedding at a shallow angle and locally cuts interbed cleavage seams. (D) Interbed cleavage seam (C1) cutting grainstone at nearly a right angle to bedding. Small, nearly vertical intrabed cleavage seams (C2) make an acute angle with bedding.

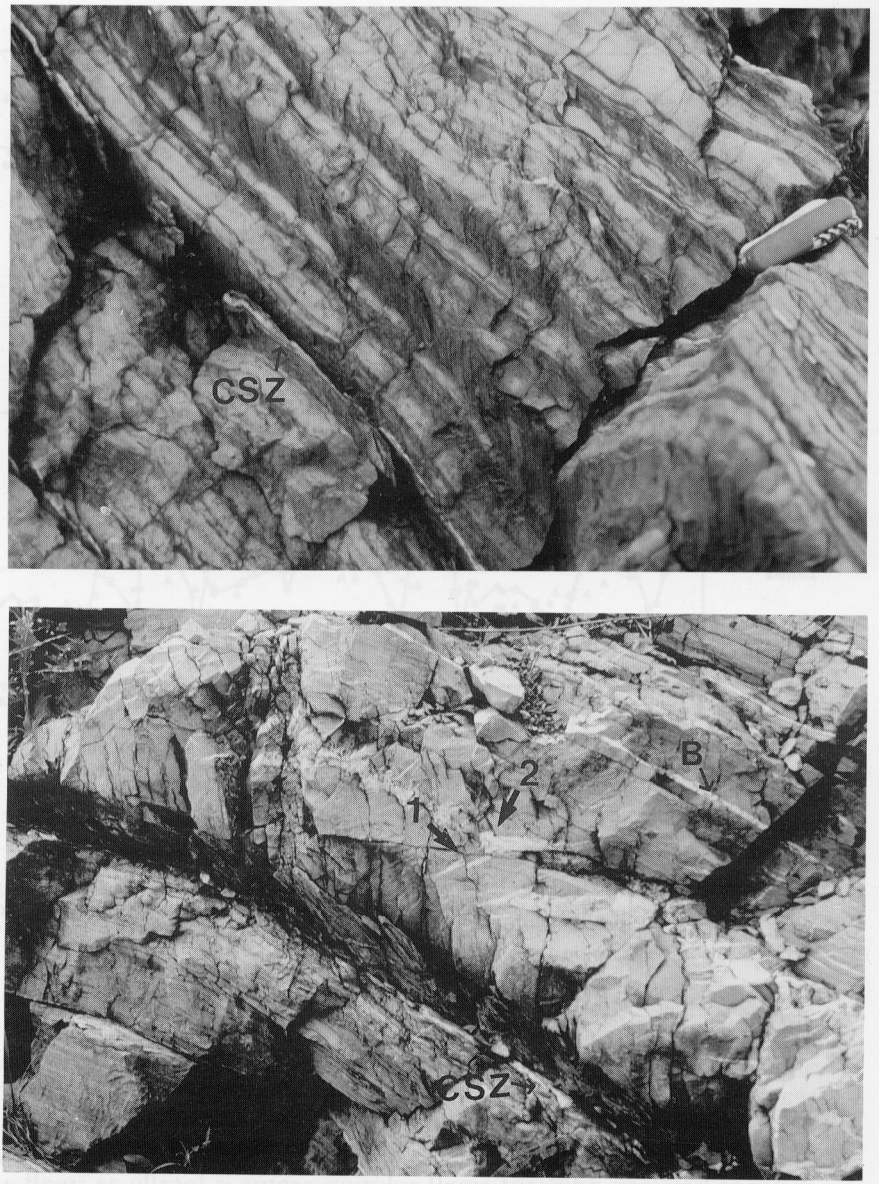

Fig. 4(E) Interlayered mudstones and grainstones cut by intrabed cleavage; cleavage cuts grainstones at high angles to bedding and mudstones at low angles to bedding. Cleavage-slip zone (CSZ) runs from upper left to center of the base of photograph. (F) Layer bounded at top by a bedding-parallel slip surface (B) and at bottom by a cleavage-slip zone (CSZ) deforms approximately homogeneously by local removal of minerals across solution seams and reprecipitation of calcite in veins. The top-to-the-left shear is consistent with flexure folding. Location 1 shows vein cross cut by an intrabed cleavage seam. Location 2 shows vein cutting across an intrabed cleavage seam.

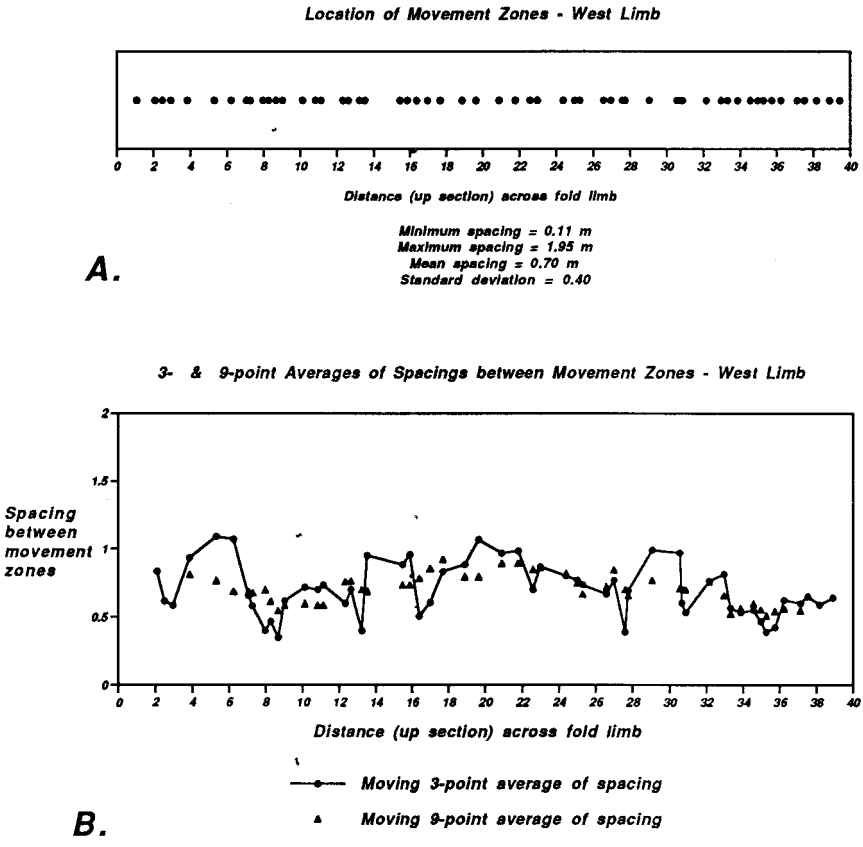

Fig. 5. Data on spacing of movement zones on east and west limbs of the fold. (A) Plot showing stratigraphic position of movement zones on west limb; open circles denote location of movement zone. (B) Plots of 3- and 9-point moving averages of spacing between movement zones versus position across western fold limb.

anastomosing habits (Engelder and Marshak, 1985). Interbed cleavage seams are very regularly spaced in individual beds, with only slight decreases in the distance between adjacent seams near the anticline hinge. In grainstones, spacing is typically about 0.5 m; in mudstones, the distance between adjacent small solution seams is locally as small as 10 cm. Offsets of bedding and truncations of fossils indicate that individual seams record losses of 5 mm to 5 cm of material measured normal to the seam. In thin section, the thick selvage accumulations along interbed cleavage seams lack a platy appearance, indicating low clay content. These accumulations probably contain more organic debris than detrital material.

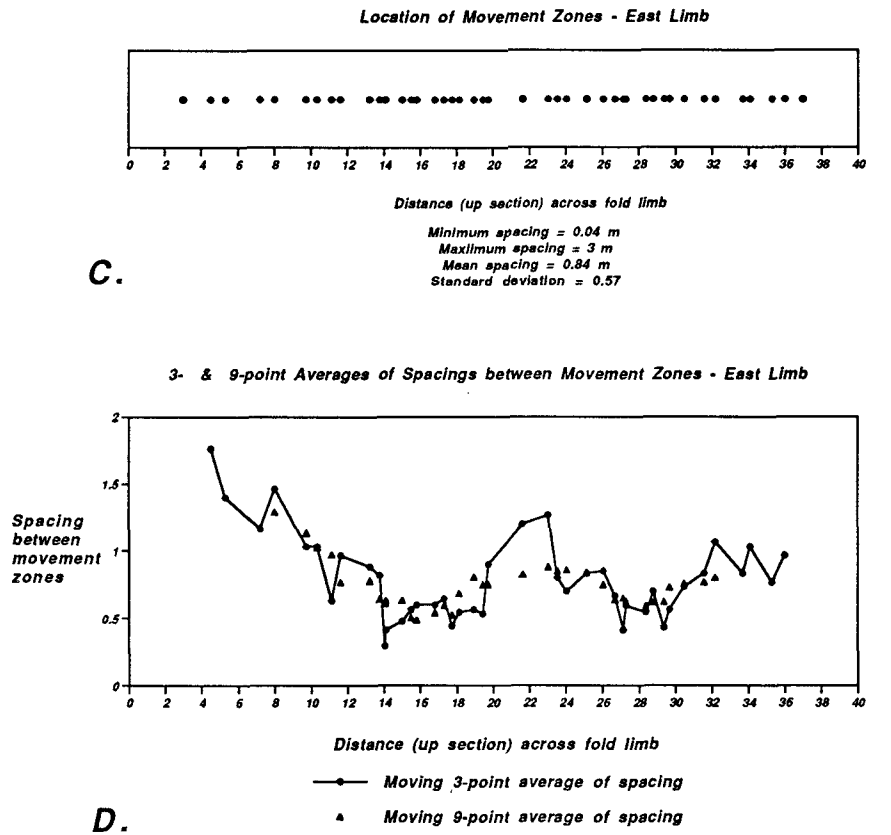

Fig. 5(C) Plot showing stratigraphic position of movement zones on east limb; open circles denote location of movement zone. (D) Plots of 3- and 9-point moving averages of spacing between movement zones versus position across eastern fold limb. Origin of the abscissa is the same stratum on both limbs.

Poles to interbed cleavage surfaces define a diffuse point-maximum/girdle; the best-fit great-circle girdle through the interbed cleavage poles is inclined roughly 15° to the bedding π circle (fig. 3D). Several mesoscopic structural elements overprint the interbed cleavage. Slickensided bedding surfaces and minor contractional faults in movement horizons typically cut and offset interbed cleavage seams (fig. 4B and C). In grainstones, extensional veins oblique to interbed cleavage seams cut them disjunctively in some locations, while elsewhere interbed cleavage seams opened and filled with fibrous calcite. In mudstones, a second cleavage overprints and locally obscures interbed cleavage. Interbed cleavage formed, therefore, before folding or early in the evolution of the folds. Interbed cleavage accounts, on average, for 10 percent layer-parallel shortening of grainstones. We found few early bedding-parallel

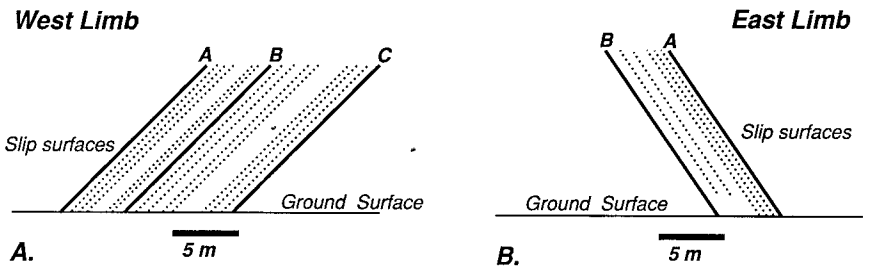

Fig. 6. Representation of movement zones identified at equivalent stratigraphic positions on the west limb (A) and east limb (B) of the anticline at the east end of figure 2. Movement zones are defined by calcite slip fiber packets. **A** denotes a prominent cleavage slip zone. **A** has a total thickness of 6 to 7 cm on each limb, with calcite fibers whose aggregate thickness is ≥ 1 cm. Bedding slip zone **B** denotes a prominent 2 to 3 cm thick calcite slip fiber packet, also found on both limbs. Also shown in (A) is bedding slip zone **C**, which has no exact equivalent on the east limb. The aggregate thickness of calcite fibers in **C** is also ≥ 1 cm. The dashed lines denote calcite fiber packets typically 1 to 2 mm thick and never, even in steps, thicker than 5 mm. Note that the spacing between thick fiber packets is greater than the spacing between thin fiber packets. Note also that the spacing of thin calcite fiber packets is not the same on opposing limbs even when equivalent thick fiber packets have formed. In (B), note two calcite fiber packets terminate laterally. Intrabed cleavage is especially well developed in the strata below their tip points, indicating that the offset accommodated as interlayer slip on the fiber-coated bedding surfaces is accommodated as intralayer flow by cleavage development.

veins and no early cross-fold veins (Srivastava and Engelder, 1990) in the strata we describe in detail here, so we infer that the material removed across the early interbed solution seams left the system entirely. Veins approximately normal to interbed cleavage seams do occur in strata nearer the base of the Silurian Tonoloway Limestone exposed in other ~200 m wavelength folds a short distance from the outcrops we describe in detail here. Those veins are cut and offset by bed-parallel slip surfaces related to fold formation and probably originated before folding began. We were, however, unable to identify comparable veins in the strata where we measured strain and volume change.

Intrabed cleavage.—The second cleavage consists of closely-spaced, wavy to anastomosing (Engelder and Marshak, 1985) solution seams consistently inclined to bedding (fig. 4C, D, and E). In thin section, these seams are rectilinear or planar (Engelder and Marshak, 1985). With a nearly constant inclination relative to bedding in each limb, this cleavage is axially planar or fans divergently (Ramsay, 1967, p. 405). Although seams with comparable orientations often occur in adjacent beds, individual seams rarely cross primary bedding. We call this cleavage, therefore, *intrabed cleavage.*

Poles to intrabed cleavage surfaces also define a diffuse point-maximum/girdle. The intrabed cleavage great circle coincides more nearly with the bedding π circle (fig. 3C). Intrabed cleavage seams and some veins crosscut each other (fig. 4F). Where seams cut preexisting veins, restoring missing vein segments to infer the original vein attitude

shows that intrabed cleavage seams originated at 45° to 75° angles to bedding. In mudstones, where organic components and smaller grain sizes caused solution transfer to proceed readily (Engelder and Marshak, 1985; Marshak and Engelder, 1985), intrabed cleavage is the dominant fabric. In grainstones, intrabed cleavage seams occur in close association with interbed cleavage seams, which constitute the dominant fabric.

Solution transfer across intrabed cleavage seams accommodated significant bed-parallel shear. The sense of shear is consistently top-toward-the-anticlinal-hinge. Where mudstones experienced bed-parallel shear, subparallel intrabed cleavage seams linked to form a flaggy, disjunctive cleavage (Marshak and Engelder, 1985) inclined to bedding. In these cases, intrabed cleavage may account for as much as 15 percent shortening oblique to bedding and as much as 15 percent volume loss in the affected strata (table 1). In interlayered thin grainstone and thin mudstone beds, layer-parallel shearing occurred preferentially by solu-

TABLE 1

Strain data from fold in figure 7

	sample #	limb dip	axial ratio	area ratio	β	λ′2	λ′1	mean values by limb
west limb								
a	91103	-20	1.07	0.86	15	1.25	1.09	
b	91102	-12	1.03	0.97	90	1.06	1	mean axial ratio=1.16
c	91104	-14	1.15	0.86	20	1.34	1.02	variance=0.04
d	91101	-22	1	1		1	1	
e	89120	-24	1.08	0.82	0	1.31	1.14	mean area ratio=0.88
f	91105	-28	1.12	0.87	24	1.29	1.03	variance=0.01
g	91106	-45	1.6	0.81	11	1.57	0.91	
h	91107	-44	1	1		1	1	
i	89122	-44	1.52	0.65	19	2.34	1.01	
j	91108	-48	1.11	0.88	25	1.26	1.02	
k	91109	-66	1.09	0.95	23	1.15	0.96	
east limb								
m	89114	28	1.27	0.64	22	2	1.24	
n	91110	44	1.26	0.81	-22	1.55	0.98	mean axial ratio=1.23
o	89109	44	1.11	0.77	-19	1.44	1.17	variance=0.02
p	91111	57	1.32	0.73	-20	1.8	1.03	
q	89105	56	1.08	0.79	-8	1.36	1.17	mean area ratio=0.78
r	91112	57	1.22	0.82	-20	1.5	1	variance=0.01
s	91100	58	1.27	0.73	-12	1.75	1.08	
t	91113	59	1.13	0.87	-10	1.32	1.03	
u	89102	59	1.47	0.86	-6	1.71	0.79	
v	89101	47	1.35	0.74	0	1.85	1	
w	91114	47	1.07	0.9	-21	1.18	1.04	

Locations **a** through **w** denote positions in fold. Axial ratios and area ratios calculated from measured principal valuesof the quadratic elongations. λ'_1 and λ'_2; β is the acute angle between the trace of bedding and the elongation direction (that is λ'_1 direction), with counterclockwise angles reckoned positive. Because intrabed cleavage accommodates most of the measured strain, λ'_1 is oriented appproximately parallel to the trace of intrabed cleavage; the angle β approximates the angle between intrabed cleavage and bedding.

tion removal within mudstone laminae, rotating seams toward parallelism with bedding and reducing both the thickness of mudstone laminae and rock volume (fig. 4E and F). After significant bed-parallel shear strains, solution seams in mudstones rotated through 45° or more to form thick selvage layers parallel to bedding. The mechanism we invoke to form these thick bedding-parallel selvage layers is not rotation of passive markers in simple shear zones, for passive markers rotate into parallelism with shear zone boundaries only when the angular shear strain is infinite ($\gamma = \infty$). In these mudstone laminae, cleavage planes were solution seams (active loci of dissolution) throughout their history. With some component of flattening across the zones, only modest shear strains are needed to rotate intrabed selvage seams to orientations parallel with mudstone/grainstone laminae (zone boundaries) (Ramsay, 1980). Some rotated selvage seams later became the loci of discrete, bed-parallel slip. Calcite slickenfibers commonly coat rotated selvage seams, indicating a local evolution from flexural flow to flexural slip as folding proceeded. We call the layers where this sequence occurred *cleavage-slip zones.* In some cases, the most prominent lineations in cleavage-slip zones are ridges and grooves (Means, 1987) on the bounding surfaces between strongly cleaved limestone and thick packets of secondary calcite. Slip normals determined using cleavage-slip zone normals and ridge-and-groove lineations cluster at a point maximum coincident with the pole to the bedding π circle (fig. 3B), supporting the inference that cleavage-slip zones formed during fold growth.

At one location (fig. 6B), a sequence of interlayered grainstones and mudstones containing two slickensided surfaces gives way down-dip to a stratigraphically equivalent sequence of folded layers cut by very well developed solution cleavage oblique to primary bedding and roughly axial planar to the small folds. Interlayer slip on discrete movement horizons and distributed flow by intrabed cleavage development occurred simultaneously at different positions in this stratigraphic sequence during folding. The simultaneous occurrence of flexural slip and flexural flow at different positions in this stratigraphic sequence underscores that these two processes are kinematically equivalent and are, under the appropriate conditions, interchangeable. The temporal progression from flexural flow to flexural slip in the cleavage-slip zones described above suggests that the relative contribution to the total deformation made by each mechanism may have varied over time.

Veins.—Individual planar calcite-filled veins and en echelon arrays of planar to sigmoidal veins occur throughout the folds. Veins, particularly the en echelon arrays, are especially common near the hinge of the anticline. Planar veins typically have very large length-to-width ratios, whereas veins in en echelon arrays have length-to-width ratios that approach 2:1. In both vein types, mineral fillings are syntaxial calcite fibers with rare crystals of fluorite. Blocky calcite replaces syntaxial fibers near the centers of the thicker veins, indicating either recrystallization of mineral fibers or accelerated opening of the vein. Where cleavage seams

cross veins, fibers bend or twin. Lenses or knots of selvage sometimes occur where large solution seams cut across large veins. These selvage lenses may represent wall-rock or early cleavage inclusions in veins that were subsequently pressure-solved when solution seams cut the veins.

Poles to individual planar veins with large length-to-width ratios (typically $\gg 10{:}1$) define a diffuse great circle whose pole lies near the hinge surface but plunges to the south, inclined nearly 30° to the fold axis (fig. 3E). The mutually cross-cutting relationship of some veins and the fold-related intrabed cleavage suggests that those veins and that cleavage formed at the same time. The origin of those planar veins is unclear, however. The occurrence of veins coeval with the early (interbed) cleavage in Tonoloway strata nearby suggests that there is an earlier generation of veins, initially roughly perpendicular to the early cleavage solution seams, in these strata as well. We were, however, unable to distinguish different generations of planar veins on the basis of their orientations, on differences visible in thin section, or on differences in cathodo-luminescence.

En echelon arrays of planar and sigmoidal veins occur mainly near the hinge of the anticline. The vein arrays range from 10 cm to 3 m long, with individual veins anywhere from 3 to 30 cm from vein tip to vein tip. The longest individual veins have sigmoidal shapes and curved mineral-fibers indicating that veins rotated relative to elongation directions during vein opening (Durney and Ramsay, 1973). Vein arrays that extend large distances across the outcrop appear in two settings. First are vein arrays where (1) the midpoints of the individual veins lie in a single bedding-parallel surface, and (2) these veins are normal to intrabed (late) cleavage seams and record finite extension normal to the shortening across cleavage surfaces. These large vein arrays record layer-parallel shear and formed during folding. Second are arrays where the midpoints of component veins define up-dip or down-dip extensions of minor faults cutting grainstones. Such large vein arrays cut across other structures and accommodate offset produced by broken hinge faults and limb thrusts. They may have formed during the late stages of folding, perhaps during late flattening of the fold. Both large vein arrays locally account for dilations of more than 10 percent. Volume increases due to vein formation near the anticline hinge mediate volume losses associated with cleavage formation there but do not compensate for volume losses in the limbs.

Deformation microstructures.—The occurrence of twin lamellae in the larger detrital calcite grains and in many calcite fibers in veins indicates that deformation twinning contributed to deformation. Because of the predominantly small grain sizes in most strata and the inferred non-coaxial deformation in these strata, however, we did not attempt to use twinned calcite strain measurement techniques to assess the contribution of deformation twinning to the development of the folds. Undulose extinction visible in the larger calcite grains indicates that dislocation creep also contributed to deformation. This observation is consistent with

the inferred deformation conditions. With at least 3 km of stratigraphic cover (de Witt and Colton 1964; Perry and de Witt, 1977), overburden pressure for these Silurian strata was at least 80 MPa during deformation. Temperatures may have been as high as 250°C (Mitra, 1987). Thus, intracrystalline plasticity should have contributed to deformation of calcite (Schmid, Boland, and Paterson, 1977). Because of the predominantly small grain sizes in these strata, the net importance of intracrystalline deformation mechanisms is also difficult to assess.

STRAIN MEASUREMENTS

The structures and microstructures described above, like those found in any naturally deformed rock, reflect displacement field gradients developed over a wide variety of length scales. The most common deformation elements in these rocks (solution seams, veins, or small faults) record abrupt differences in net displacement at different positions. Discontinuously deformed rocks, where total displacements change abruptly with position, may deform homogeneously at a scale larger than the scale of the individual structural elements if those elements are regularly spaced and show regular offsets (Arthaud, 1969; Wojtal, 1989). In order to measure strains in such rocks, one must determine a length scale over which displacements vary smoothly, that is, a length scale at which displacement field gradients have roughly constant values (Wojtal, 1989). We applied a strain-measurement technique designed to accommodate the discontinuous nature of the mesoscopic deformation in these strata and to measure the hand-sample scale strain. We used samples cut parallel to the fold profile plane to draw displacement diagrams, estimate displacement gradients, and calculate finite strains (see app. 1). Figures 7 and 8 and table 1 summarize our finite strain data.

Cleavage seams and veins here are evenly spaced and show consistent offsets (fig. 4D and F) within large individual hand samples, so that they accommodate locally homogeneous strains at a hand sample scale. We measured strain on individual hand samples that contain only intrabed (late) cleavage seams and veins. Thus, the strain measurements we report reflect strains developed within individual layers during fold growth (that is, flexural flow) but do not record either the early layer-parallel shortening or the bedding slip surfaces (flexural slip) that contributed to fold growth.

The occurrence of numerous diagenetic stylolites indicate that these strata had little or no porosity before deformation. The ratios of the area of sections after finite deformation to their area before finite deformation calculated from strain data (table 1) thus provide an estimate of the area change in the profile plane during deformation (assuming no significant transfer of material or reprecipitation is hidden in pore cavities). Examination of bedding surfaces on the outcrop and of sawcut faces in hand samples indicates that the mesoscopic cleavage seams and veins that accommodated strains are all roughly orthogonal to the profile plane for this fold and to the plane of section for the individual samples (fig. 3A, B,

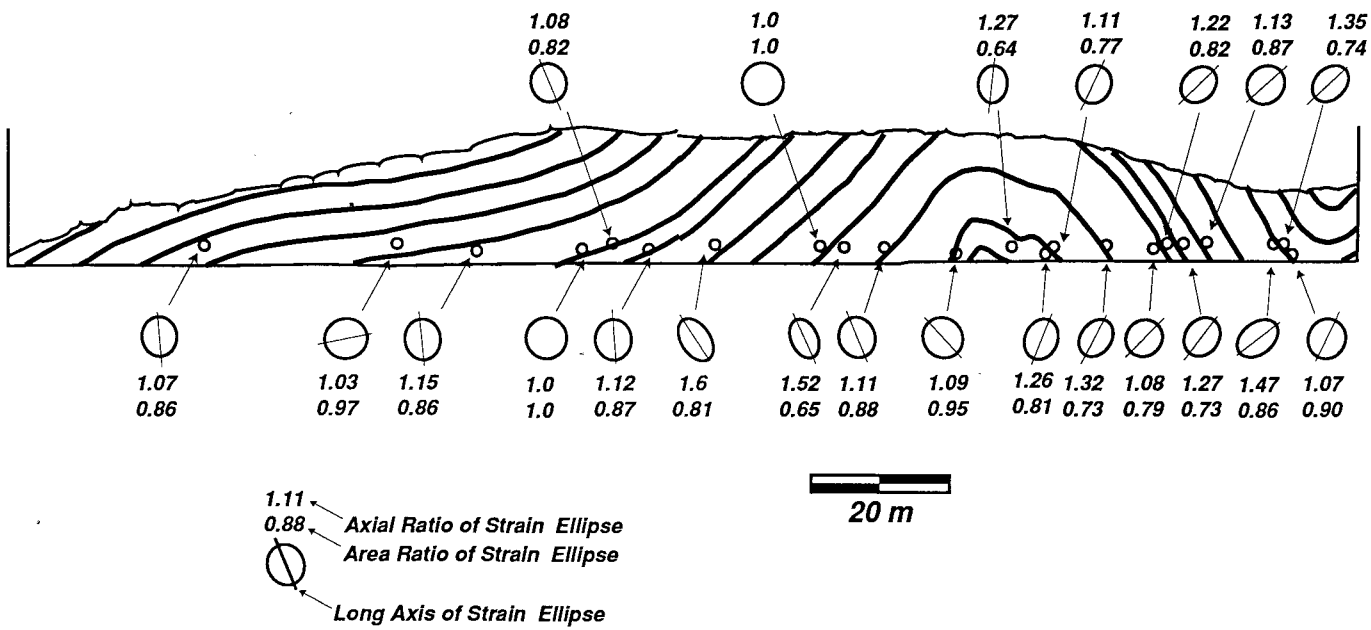

Fig. 7. Detailed profile of folds in the Silurian Tonoloway Limestone (indicated on fig. 2B), drawn on a plane whose normal is 028, 07, showing locations of samples for strain measurements and strain data. Ellipses denote strain magnitudes and orientations at locations **a** through **w** (from west to east); strain axial ratios and area ratios given in table 1. Finite strain data record the intralayer deformation accommodated by veins and intrabed cleavage solution surfaces (flexural flow). They do not record the early layer-parallel shortening accommodated by the interbed (early) cleavage solution surfaces (pre-folding layer-parallel shortening) or the interlayer strains (flexural slip) accommodated by bedding-slip surfaces, cleavage-slip zones, or other movement horizons.

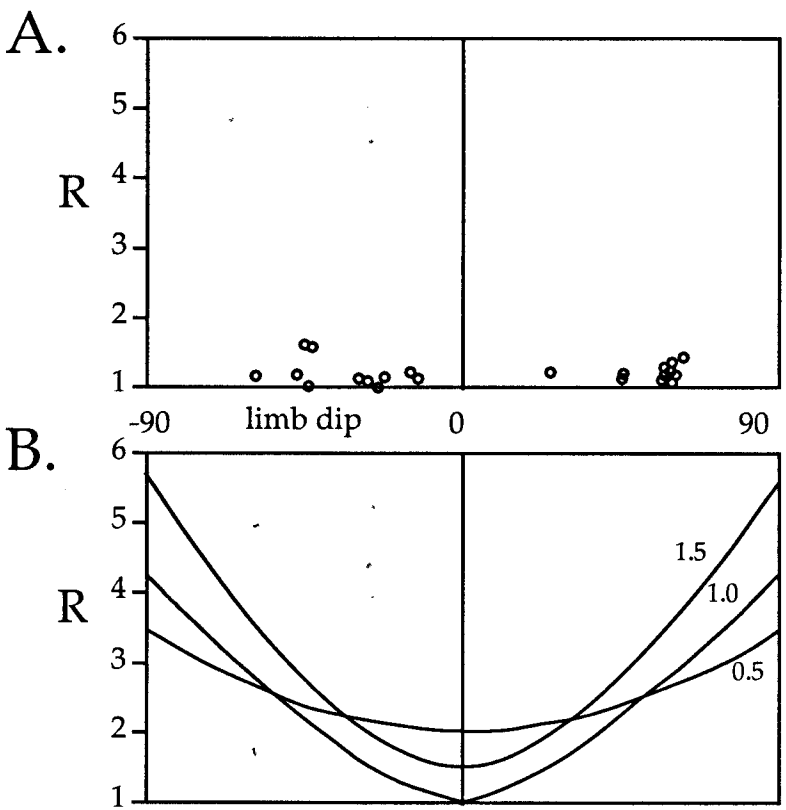

Fig. 8. Relation between axial ratio (R) and limb dip. (A) data from studied fold, taken from table 1. (B) predicted values of R for flexural folds with initial layer parallel strains, taken from Ramsay and Huber (1987, fig. 21.34); the numbers 0.5, 1.0, and 1.5 represent axial ratios of the strain ellipse before folding (R_o).

C, D, and E). During the fold-related deformation, the individual rock components had relative displacement vectors confined to the profile plane. As a result, we believe that our area ratios are good estimates of the local volume changes.

We also estimated the shortening due to removal of material on early interbed cleavage seams in two steps. First, we measured the mean spacing of these interbed cleavage seams in the nearly flat-lying strata west of the anticline hinge and assumed that this spacing estimates the original spacing of these cleavage seams. Second, we determined the average offset across the seams by measuring the offsets of sedimentary layers and/or by comparing the concentration of insoluble material in seams to the concentrations of insoluble minerals within the adjacent limestone. Both types of measurements indicate that the formation of the

early interbed cleavage seams accounted for ≥ 10 percent layer-parallel shortening.

The growth of the 150 to 250 m wavelength folds accommodated additional mesoscopic subhorizontal shortening of these strata. We measured the horizontal distance between the eastern anticlinal hinge and the westernmost anticlinal hinge on figure 2 to estimate the present length of strata exposed here. We measured the arc length of an identifiable sedimentary sequence in our detailed profile in order to estimate the original length of the strata here. The present length of these strata is 0.82 of the pre-folding length, indicating that mesoscopic fold growth resulted in 18 percent shortening of the strata.

DISCUSSION

Cleavage formation and volume loss during deformation.—This fold exhibits both convergently and divergently fanned (Ramsay, 1967, p. 405) cleavages. Cleavages in folds often originate before folding as bed-normal solution seams (Alvarez and Engelder, 1976; Alvarez, Engelder, and Geiser, 1978; Helmstaedt and Greggs, 1980; Engelder and Marshak, 1985; Marshak and Engelder, 1985; Henderson, Wright, and Henderson, 1986; Meyer and Dunne, 1990). With fold growth, such an early cleavage may rotate passively with the limbs to produce a convergent fan. In less competent beds, shearing of the early cleavage can produce divergently fanned cleavage. Here, however, three lines of evidence indicate a different mechanism for cleavage genesis (fig. 9).

First, poles to intrabed cleavage and interbed cleavage define two different point maxima (fig. 3C and D). There are two possible reasons for their non-coaxial geometries: (1) early shortening occurred on preexisting joint surfaces that bear no relation to folding, or (2) early cleavage seams developed in response to a shortening event that was non-coaxial with folding. If joint surfaces oblique to the maximum shortening direction accommodate shortening by pressure solution, stylolitic teeth develop at oblique angles to the surface (Arthaud and Mattauer, 1969; Dean, Kulander, and Skinner, 1989). The orientation of stylolitic teeth normal to interbed cleavage surfaces supports the second explanation, that the early shortening direction was not parallel to the shortening accommodated by folding.

Second, bed-parallel movement horizons, minor faults, and veins consistently overprint the *interbed* cleavage, indicating that this cleavage formed before finite-amplitude folding (fig. 4B, C, and D). Third, crosscutting relationships support the formation of *intrabed* cleavage during folding. This later *intrabed* cleavage exhibits mutually crosscutting geometries with the veins and movement horizons. Restoring veins offset by intrabed cleavage to planar orientations shows that intrabed cleavage surfaces formed at oblique angles to bedding (with a different sense of obliquity on either side of the fold axis) in orientations inconsistent with pre-folding layer-parallel shortening.

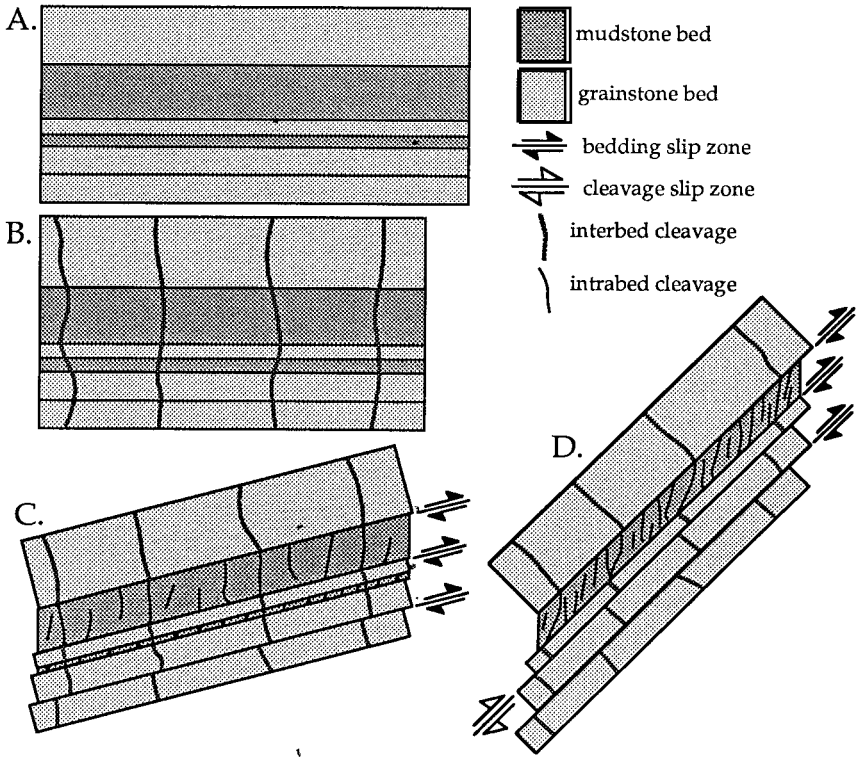

Fig. 9. Schematic representation of the relationship between interbed and intrabed cleavage, bedding-slip zones, and cleavage-slip zones. (A) Undeformed strata. (B) Deformation during layer parallel shortening (before fold amplification). (C) Deformation during low amplitude folding. (D) Deformation as fold reaches maturity.

Intrabed (late) cleavage is compatible with the fold geometry and other fold-related structures, whereas the interbed (early) cleavage is not (fig. 3C, D, and G). The two cleavages represent two distinct shortening events (fig. 9). Bed-normal interbed cleavage formed before folding, accommodating layer-parallel shortening. In competent beds (grainstones), interbed cleavage surfaces rotated more or less passively during folding, remained normal to bedding, and are well-preserved. In less competent strata (mudstones), the later intrabed bed cleavage overprinted the earlier cleavage. Intrabed cleavage is not well-developed in most grainstone beds, so some other mechanism must account for the additional shortening of these layers. In the hinge of the fold (fig. 4A), minor faults shortened a single grainstone bed. These faults resemble the limb thrusts in chevron folds described by Ramsay (1974), suggesting that grainstone beds were shortened by mechanisms comparable to those experienced by relatively thick beds in chevron folds. Limb thrusts,

bulbous hinges, and passive rotation to steeper limb dips (Ramsay, 1974) could, then, account for lower strains in grainstones during folding.

Strain data presented above indicate layer-parallel shortening of 10 percent due to the formation of the early interbed cleavage seams with an additional 18 percent shortening due to fold growth. Formation of the late intrabed cleavage accommodated between 10 and 15 percent shortening oblique to layering. In the case of the cleavage-accommodated strains, these shortening measurements estimate the volume of rock lost during deformation. Total sub-horizontal shortening of these strata is, at a minimum, that due to the early interbed cleavage plus that accommodated by fold growth; these strata experienced at least 25 percent sub-horizontal shortening (fig. 10). The later intrabed cleavage probably accounts for additional sub-horizontal shortening, although it is difficult to quantify exactly how much this cleavage contributed to regional shortening. We completed a sequential restoration of the folded and cleaved strata here to provide one estimate, and our restoration indicates that all structural elements in these strata accommodated at least 32 percent shortening (fig. 10). The total subhorizontal shortening accommodated by the deformation elements we mapped could be 35 to 45 percent if the early cleavage accommodated more layer-parallel shortening (fig. 10).

Buckling versus bending origin for the folds.—Folds and faults in the central Appalachian Valley and Ridge Province, like folds and faults in other fold-thrust belts, are inherently interrelated. In such settings, it is important to determine the extent to which bending (folding due to moments applied across a layer) versus buckling (folding due to instabilities that arise during compression along the length of the layer) contributed to fold initiation and growth (Hudleston, 1986). Isolated folds in homogeneous, unfaulted media (Currie, Patnode, and Trump, 1962; Woodward, 1992) and detachment folds far above a fault (Mitra, 1992) probably form mainly by buckling. Fault-bend folds (Suppe, 1983, 1985) form mainly by bending. In fault-propagation folds (Suppe, 1985; Jamison, 1987), both bending and buckling contribute to fold growth. Many fault-related folds are demonstrably not either simple fault-bend or simple fault-propagation folds (Fischer and Woodward, 1992; Fischer, Woodward, and Mitchell, 1992).

The geometric setting of a fold in relation to other structures is of primary importance in determining the origin of that fold; fault-related folds must be specifically linked geometrically and kinematically to faults. In the folded Siluro-Devonian cover strata we describe here, folds are not simple fault-bend folds above ramps in faults. There are no major thrusts mapped in the cover strata, and the few faults recognized have neither the appropriate positions, the correct geometry, nor the correct scale to give rise to the observed folds. It is, however, difficult to rule out entirely a bending contribution to fold growth. Although mapped thrust faults in cover strata are rare, the folds described here might have initiated by a

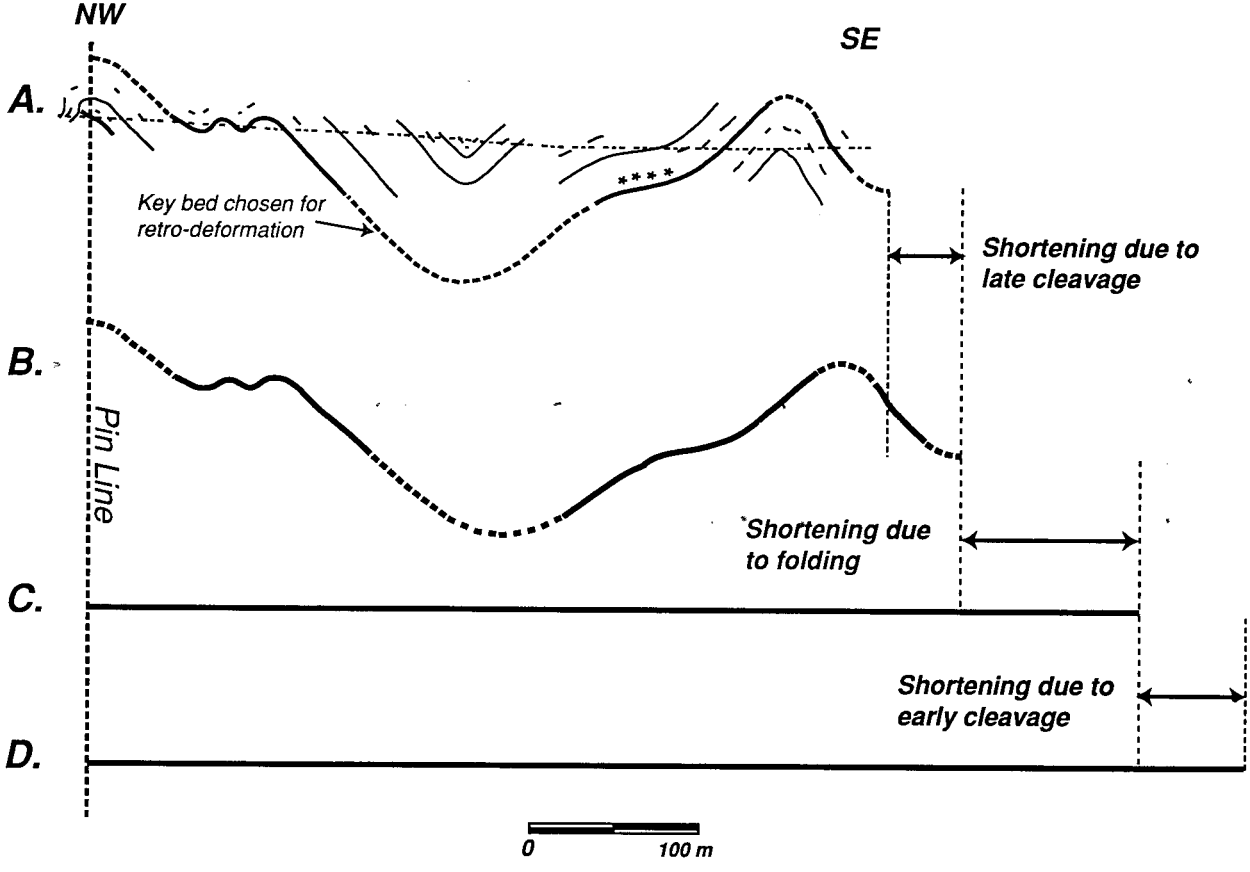

Fig. 10. Sequential restoration of folded strata. (A) Present state profile. (B) The key bed after unstraining to undo the effects of the late (interbed) cleavage. We used the mean values of strains measured on the east limb to determine the change in length and rotation of the key bed on the east limb. We used the mean values of strains measured on the west limb to determine the change in length and rotation of the key bed on the west limb. We used the lower strain values (those on the west limb) to unstrain other portions of the key bed but did not change the lengths of those portions of the bed lacking the later (intrabed) cleavage (for example, the segment denoted with asterisks). (C) The key bed unfolded. (D) The length of the key bed with the effects of the early (interbed) cleavage removed. We conservatively estimated shortening due to the formation of the early cleavage as 10 percent. Comparing the length of the key bed in (A) and in (D), we find 32 percent total shortening.

combination of buckling and bending associated with fault tips (Jamison, 1987) within the cover strata.

Several features indicate a buckling origin for the folds we described here. Folds in these Silurian strata have regular wavelengths (de Witt and Colton, 1964; fig. 2). These folded strata are interlayered limestone and dolomitic grainstones and mudstones in the central portion of the Tonoloway Limestone, which has sizable thicknesses of shaly strata at the top and bottom of the unit (de Witt and Colton, 1964). This stratigraphic setting of an isolated resistant unit embedded in less resistant units is consistent with a buckling origin (Currie, Patnode, and Trump, 1962). Using measured thicknesses of limestones and dolostones in the central Tonoloway Limestone (de Witt and Colton, 1964), the wavelength-to-thickness ratio for the fold is about 5:1. This ratio lies within the range of predicted (Smith, 1979) ratios for wavelength to thickness in buckle folds.

A southeast-dipping fault with relatively small offset cuts strata in the core of an overturned anticline in the train of folds approx 250 m to the west of the anticline described in detail here (fig. 2), but no major faults cut these folded strata. Mesoscopic structures such as the limb thrusts (fig. 4A) and the distribution of late cleavage-related strains (fig. 7) indicate that the fold developed from an initially rounded shape to its present angular, flattened shape (fig. 10). In addition, several mesoscopic and microscopic structures indicate that the hinge was "pinned." Movement horizons cut and offset early interbed cleavage seams with a consistent sense of offset of top-toward-the-anticlinal-hinge on both fold limbs (fig. 4C and D). The intrabed cleavage seams that curve asymptotically into parallelism with cleavage-slip zones show also consistent top-toward-the-hinge offsets on both limbs (fig. 4C and F). Mineral fiber steps on movement horizons and in cleavage-slip zones agree with this inferred sense of offset. Movement zones that lack associated intrabed cleavage or offsets of interbed cleavage cut up section toward the anticlinal hinge, suggesting that offsets were consistently top-toward-the-anticlinal-hinge (compare fig. 2 in Tanner, 1992). In addition, strains associated with the intrabed cleavage agree with top-toward-the-anticlinal-hinge shear on both limbs (figs. 7 and 8; table 1). If this fold formed within a setting of top-to-the-west shearing, this shearing must be accommodated by variations in fold shape (fig. 2; Dubey and Cobbold, 1976) or in the distribution of strains within the fold (Manz and Wickham, 1978), not by the development of a rolling hinge or by the development of any sizable through-going faults. Fischer, Woodward, and Mitchell (1992) argue that most models for pinned hinge folding predict a concentration of strain in the area near the axial surface, although this fold shows no such strain concentration (figs. 7 and 8). Nonetheless, an inference of a buckling origin for this anticline is reasonable.

It is possible that the folds described here initiated and grew as buckle folds above detachments in the cover strata under conditions other than homogeneous horizontal shortening within the cover strata (see fig. 13 in Geiser, 1988b). In this case, some of the slip between major

horses in the imbricated Cambro-Ordovician strata would have been partitioned into either distributed layer-parallel shearing or minor faults in the cover strata (Perry, 1978; Kulander and Dean, 1986; Mitra, 1986). Top-to-the-west shear distributed across the cover strata need not produce markedly different thicknesses of the limbs of folds in these strata nor generate significant asymmetries in the strains in opposing limbs (Manz and Wickham, 1978), but it could have contributed to the overturned shapes of folds in these strata (Meyer and Dunne, 1990).

Single-layer (flexural flow) versus multi-layer (flexural slip) behavior.—During the initial stages of deformation, the strata in this fold probably behaved as a coherent unit defined by the stratigraphic extent of a pinned hinge. Fold amplification required a significant amount of layer-parallel shearing, either by slip on discrete surfaces or within narrow zones, as flexural slip, or by shear distributed across wider layers, as flexural flow (Tanner, 1989). We argue below that movement horizons and cleavage-slip zones developed at different stratigraphic positions in the different fold limbs during folding and that the spacing of movement horizons changed during folding. We infer that these changes caused a transition in the rheological behavior of the stratigraphic package during fold growth.

The bed-normal spacing between the thick slickenfiber packets in movement horizons or cleavage-slip zones is greater than the bed-normal spacing between movement horizons or cleavage-slip zones composed of thin slickenfiber packets (fig. 6). If slickenside thickness correlates with the length of time that each surface remained active and if slip on all beds ceased at about the same time, the later stages of folding entailed flexing increasingly thinner packets of beds. This transition to multi-layer folding effectively isolated successively thinner beds as distinct rheological units. This suggestion contradicts one made by Chapple and Spang (1974), who argued that the interbed slip horizons found in an asymmetric fold that formed under comparable conditions in similar rock types were active throughout fold growth. Plots of interbed slip on fold limbs versus total shortening in one set of experiments on the growth of flexural-slip folds showed that interbed slip accrued slowly during early stages of fold growth and accelerated at limb dips of approx 30° (Behzadi and Dubey, 1980). It is plausible that an increase in the number of bedding-parallel slip zones, which also accommodated greater amounts of interbed slip, could have occurred at a comparable stage, at moderate limb dips, during the growth of this anticline.

Intrabed (late) cleavage seams accommodated layer-parallel shearing *within* individual layers in the growing fold at the same time that slip accrued on discrete bedding surfaces. The mean value of the axial ratio for intrabed cleavage-related strains on the east limb of the fold is 1.23; the mean value of the axial ratio for strains on the west limb of the fold is 1.16 (see table 1). The probability that a difference this large will occur by chance is less than 35 percent ($t = 0.95$ with 20 degrees of freedom; Lewis, 1984). The mesoscopic structures responsible for these strains are intrabed (late) cleavage surfaces, cleavage-slip zones, and veins. The

strain data are consistent with the observation that the intrabed (late) cleavage is more strongly developed on the east limb of the fold than on the west limb.

Contrary to intuition, figure 8 shows that area ratio (and axial ratio) do not correlate meaningfully with limb dip, as might be expected for the flexural-flow mechanism. This suggests that, although flexural flow contributed significantly to the development of the fold, flexural slip was the dominant mechanism active during folding. The mean spacing of movement zones, comprising bed-parallel and cleavage-slip zones, is 0.84 m on the east limb of the fold and 0.70 m on the west (fig. 5). The statistical difference between the mean spacing of movement zones on the two limbs is strong (probability $P < 15$ percent; $t = 1.51$ with 95 degrees of freedom; Lewis, 1984); we infer that the difference in mean spacing of movement horizons on opposing limbs is significant and reflects spatial variations in the contribution of flexural slip to fold development.

Variations in strain magnitudes and volume loss across limbs suggest that flexural flow made a proportionally greater contribution to fold development on the east limb. Movement horizons, which indicate flexural-slip, are more closely spaced in the west fold limb. We suggest that the differences in the spacing of bedding-parallel slip zones and the different magnitudes of intralayer strain accommodated by the intrabed (late) cleavage in the two limbs are related: the strain magnitude on each fold limb correlates inversely with the spacing of movement horizons on that limb.

As noted above, flexural slip in movement horizons and flexural flow by intrabed (late) cleavage development occurred simultaneously in different segments of the stratigraphic sequence during folding and are kinematically equivalent processes. The factor or collection of factors that influenced the local selection of one mechanism of shearing over the other during flexural folding is not known. The difference in limb-flexure mechanisms across this anticline is probably not due to differences in rock type across the fold, for very similar rock types occur on opposing limbs. It is possible that the difference between the two limbs is related to fluid-flow patterns or that it is random and has no structural or kinematic implications..

Changing the thickness of individual layers in a multi-layer package or changing the manner of coupling between those layers is likely to change the overall resistance to dynamic fold amplification for the package and its tendency to acquire a particular final fold shape (see Ramsay and Huber, 1987, p. 413-444 or Price and Cosgrove, 1990, p. 304-330 for reviews and references). First, since resistance to buckling and amplification is proportional to layer thickness, reducing layer thicknesses lowers a multi-layer package's resistance to amplification. The development of cleavage-slip horizons and the nucleation and growth of additional bedding-parallel slip zones or movement horizons during fold growth would have reduced layer thicknesses during fold growth; the pinned hinges indicate that fold wavelength remained con-

stant despite these changes in layer thickness. If far-field stresses remained nearly constant during folding, fold growth could have accelerated as cleavage-slip zones developed and/or as additional bedding-parallel slip zones or movement horizons nucleated. We noted above a significant difference in mean spacing of bedding-parallel slip zones and movement zones on the two limbs. We infer, then, that the opposing limbs of the anticline made unequal contributions to the total resistance to fold amplification. We do not believe that this changing resistance to fold amplification can be correlated directly with net limb dip in this train of folds, particularly since the relative contribution of intralayer strain (flexural flow) apparently compensates for reductions in interlayer slip (flexural slip). A decrease in the resistance to slip between layers, caused by the evolution of cleavage-slip zones, could also lead to more angular fold shapes and could enhance the development of accommodation structures in hinge regions like limb thrusts and bulbous hinges (Ramsay, 1974; Price and Cosgrove, 1990, p. 319-321). In the context of the current debate on the relative importance of regional buckling versus regional thrusting (Fischer, Woodward, and Mitchell, 1992), subtle changes in the character of folded layers could alternately lead to conditions favorable for the development of folds at the expense of thrusts or for the nucleation of thrusts across folds, such as the break thrusts of Willis (1893).

Solution transfer normally implies a linear bulk rheology (Elliott, 1973; Rutter, 1976), although significant volume losses here may indicate that the linear flow laws traditionally applied to solution transfer may be inappropriate (Etheridge and others, 1984). Significant volume loss is incompatible with closed systems where material removed from regions of high compressive stress reprecipitates in nearby areas of low compressive stress (Weyl, 1959; Elliott, 1973; Engelder, 1984; Bell and Cuff, 1989). Including advection in a solution-transfer deformation mechanism may lead to a power-law bulk rheology (Geiser and Sansone, 1981). The overprinting relations we describe in this anticline indicate a complex structural history for rocks in this fold. The type of diffusive mass transfer active in these strata and its relative importance to the growth of the fold probably changed throughout fold growth. The bulk rheology of these strata probably varied with position in the fold, akin to the situation outlined by Mitra (1978), and also probably varied significantly as folding proceeded. Thus, theoretical models of fold growth based on uniform material properties for the folded layers should not be expected to reproduce or explain all structures observed in natural folds.

CONCLUSIONS

The character, geometry, and sequence of the deformation structures and microstructures in these two hundred-meter wavelength folds support a buckling mechanism. We propose the following sequence of events:

1. Prior to tectonic deformation, strata compacted and lithified (fig. 9A). Bedding-parallel stylolites formed. Diagenesis significantly reduced porosity.

2. Strata shortened across evenly-spaced, bed-normal stylolites that form the interbed cleavage (fig. 9B). Material removed across interbed cleavage solution seams during pre-folding layer-parallel shortening left the system entirely, producing a 10 percent volume loss. This early layer-parallel shortening had a northwest azimuth.

3. Finite-amplitude folding accommodated regional shortening along a west-northwest azimuth. In other words, this shortening was not coaxial with the early layer-parallel shortening. Fold growth accounted for 18 percent shortening in this area, which added to the shortening by the early cleavage yields a minimum of nearly 30 percent sub-horizontal shortening for these strata. Two hundred-meter wavelength folds may have initiated with relatively rounded fold shapes and little variation of bed thickness. The anticline described in detail here grew mainly as a flexure fold with pinned beds at the fold hinge. Grainstones in this fold probably shortened primarily by rotating passively to steeper dips; these beds may have continued to shorten across interbed (early) cleavage surfaces. Bedding slip occurred initially on smooth primary bedding surfaces. The development of intrabed (late) cleavage seams accommodated bedding-parallel shear (flexural flow) in mudstones (fig. 9C). Mudstones and laminated mudstone/grainstones in fold limbs experienced an additional 10 to 15 percent volume loss as intrabed (late) cleavage developed.

4. With continued shortening, the fold probably acquired a more angular shape (fig. 10). Movement horizons remained active, and intrabed cleavage continued to develop. This late cleavage intensified in some beds, leading to the development of cleavage-slip zones. We infer that the bulk rheology of these strata changed as cleavage-slip zones evolved into new bed-parallel slip surfaces (fig. 9D). In the fold hinge, grainstones shortened discontinuously, forming limb thrusts (Ramsay, 1974). En echelon vein arrays nucleated and grew at the tips of these minor faults. This vein growth moderated volume losses in the hinge.

The two cleavages represent distinct, noncoaxial shortening events. Nickelsen (1988) and Gray and Mitra (1993) have documented angular rotations for the azimuths of successive shortening episodes in the Appalachian Valley and Ridge Province in Pennsylvania. An angular discordance has not before, to our knowledge, been suggested for this segment of the belt. The change in shortening direction with time that we observe here is counterclockwise, similar to that for strata about 100 km along strike to the north (Nickelsen, 1988). The sense of rotation of shortening directions observed here and in central Pennsylvania differs, however, from the sense of the rotation seen in eastern Pennsylvania (Gray and Mitra, 1993).

The total shortening experienced by these strata must be at least 25 percent (fig. 10); it may be as much as 40 percent. Much of the total

shortening occurred by removal of material across solution seams. Total volume loss of as much as 25 percent during deformation demonstrates that volume loss both before and during folding may account for some of the missing length in cover strata in balanced-cross section restorations. This volume loss also suggests that during folding a significant volume-transport system may have linked to the strata stratigraphically above and below.

ACKNOWLEDGMENTS

We thank Mary Beth Gray, Peter Hudleston, Charles Onasch, and Basil Tikoff for comments on early versions of this paper. Careful and critical reviews by Richard Nickelsen and Peter Geiser led to significant improvements in the manuscript. SFW thanks Tom Billiard and Dana Cannon for assistance in collecting additional data in the field. We used R. W. Allmendinger's program *STEREONET* for all the stereographic projections used in this paper. This work was supported by a ROA Supplement to National Science Foundation Grant No. EAR-8804670 (awarded to Dr. P. J. Hudleston) and by grants from the Oberlin College Research and Development Committee.

APPENDIX 1

Changes in shape (that is finite strains) and/or solid-body rotations result when different material points in an object have different net displacements (Elliott 1970; Ramsay, 1976). Structural geologists have devised numerous ways to measure quantitatively finite strains, but each method ultimately derives from transformation equations that relate the positions of material points in the undeformed and deformed state (Ramsay, 1976). Strain measurements normally defined as comparisons of the lengths of material lines in the undeformed and deformed states or as comparisons of angles between pairs of material lines in the undeformed and deformed states can be rewritten as functions of the spatial gradients of the displacement field. Thus, if one knows the magnitudes of the spatial gradients of the displacement field one can determine directly the magnitudes of finite strains or determine directly the orientation and shape of a representative strain ellipsoid. This approach is particularly useful when treating situations where the scale of observation is one at which the deformation is discontinuous (Wojtal, 1989).

In order to measure strains in the discontinously deformed Tonoloway Limestone, we used the following procedure. First, on a polished rock face cut parallel to the profile plane for the folds, we defined arbitrarily a set of right-handed Cartesian coordinate axes x' and y'. After locating the intersections of each deformation element (that is each stylolite seam or vein) with the coordinate axes, we used the points midway between deformation elements to denote the "positions" of blocks of rock subjected to approximately uniform displacements. We determined the reciprocal displacement of each block relative to its neighboring block along a traverse parallel to one of the coordinate axes by reconstructing layers removed by pressure solution or by rejoining layers now separated by mineral-fillings (fig. A-1A). We envision each block to be rigid, that is all points in the block have the same net displacement. This is not strictly true, of course. Following Wojtal (1989), we then constructed *displacement diagrams* to determine the net reciprocal displacements of blocks separated by several deformation elements (figs. A-1B and A-2A). For example, in figure A-1A, the net reciprocal displacement vector for block C relative to the origin block O is $\mathbf{u}'[C,O]$, the resultant of the reciprocal displacement vectors $\mathbf{u}'[A,O]$, $\mathbf{u}'[B,A]$, and $\mathbf{u}'[C,B]$

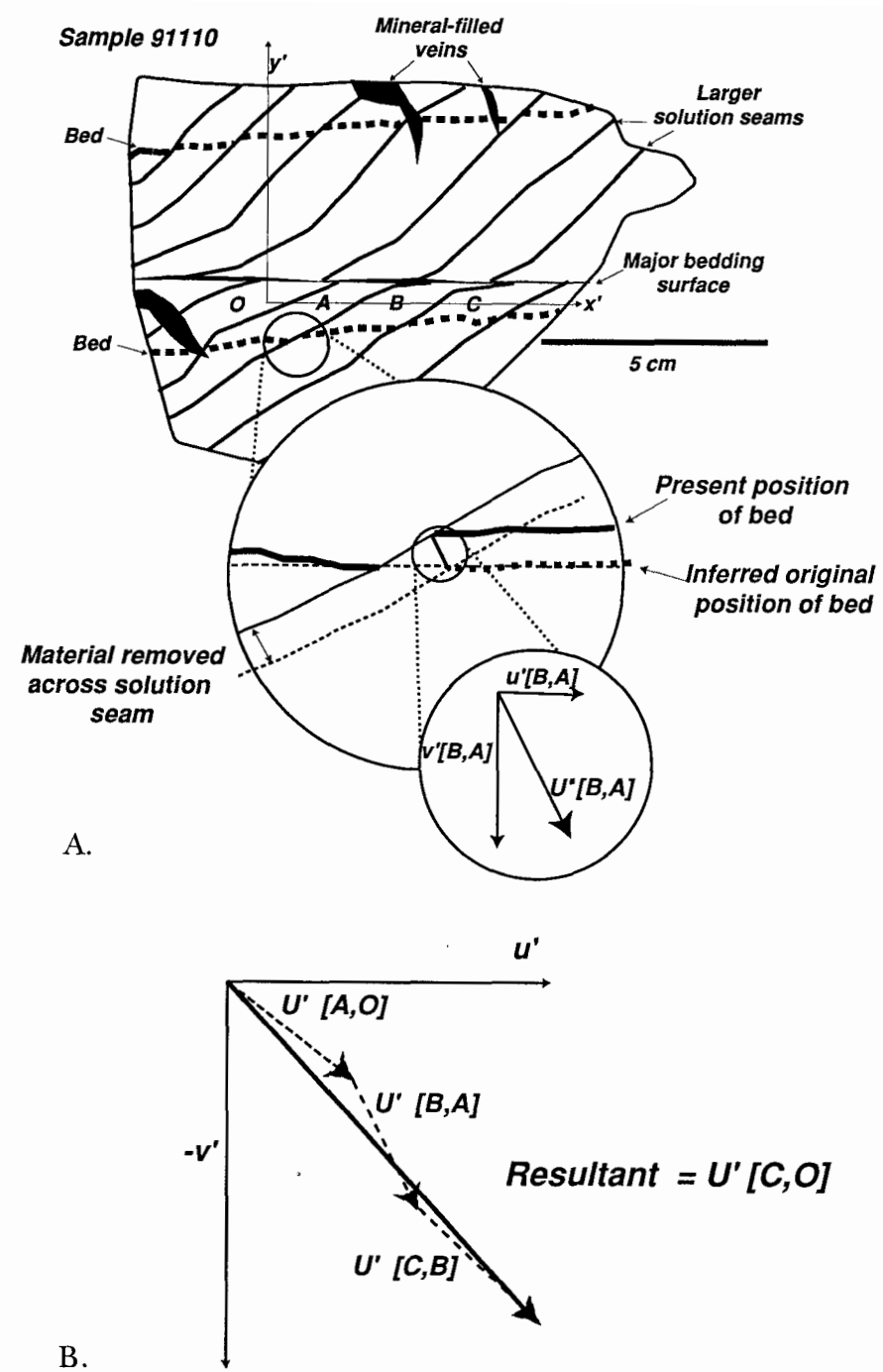

Fig. A-1(A) Sketch of polished rock face showing traces of bedding and larger solution seams and the outlines of mineral-filled veins. Cartesian coordinate axes x' and y' drawn in arbitrary orientation. A traverse along x' axis encounters blocks O, A, B, and C separated by larger solution seams; the labels A, B, and C indicate the "position" of each block along the traverse, that is (x'[B], 0) for block B, and (x'[C], 0) for block C. The first inset is an enlargement of area in the vicinity of the solution seam separating blocks A and B showing the present position of an identifiable bed and its inferred original position. The second inset shows the reciprocal displacement vector for block B relative to block A. This vector restores block B to its original position relative to block A. We resolve the reciprocal displacement into components u'[B, A] and v'[B, A], parallel to the coordinate axes x' and y', respectively. (B) Hypothetical displacement diagram showing that the net reciprocal displacement of block C relative to the origin block O is the vector sum of the reciprocal displacement of block A relative to block O, the reciprocal displacement of block B relative to block A, and the reciprocal displacement of block C relative to block B.

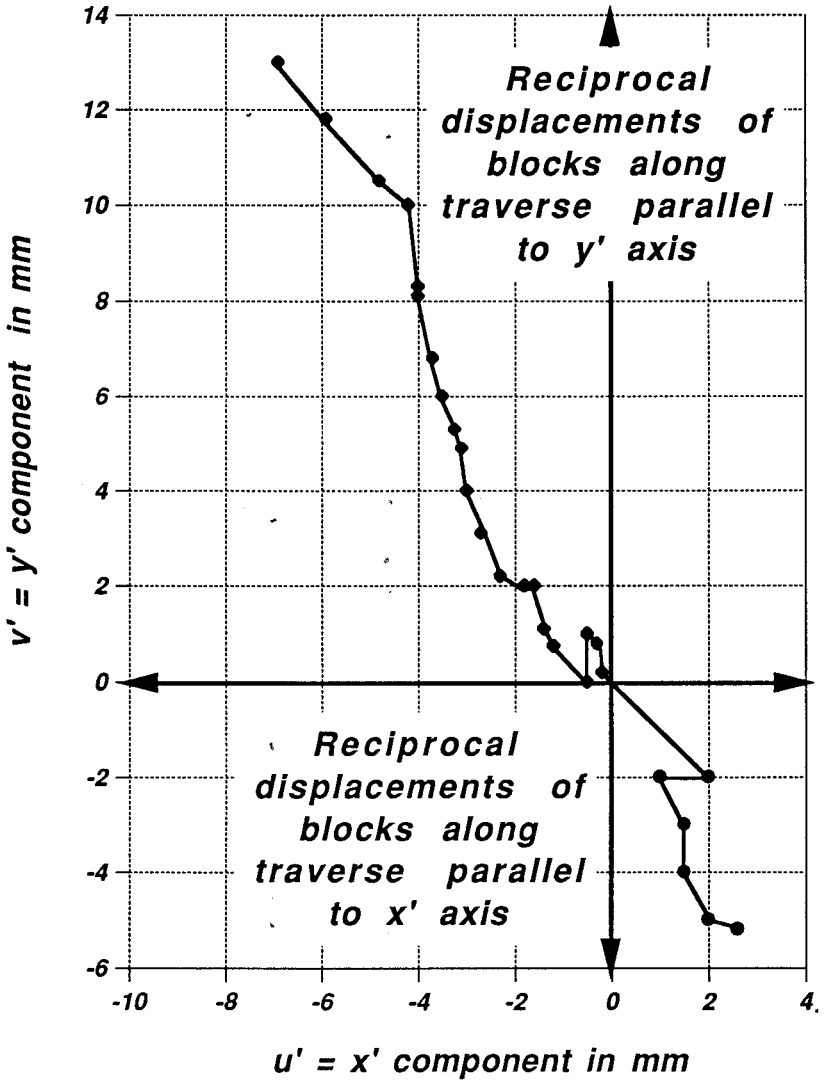

A.

Fig. A-2(A) Displacement diagram derived from traverses along x' and y' axes for sample 91110 (shown in fig. A-1(A)).

(fig. A-1B). We resolve the net reciprocal displacement vector into components parallel to the Cartesian coordinate axes. Thus

$$\mathbf{u}'[C,O], = u'[C,O]\,\mathbf{i} + v'[C,O]\mathbf{j}, \qquad \text{(A-1)}$$

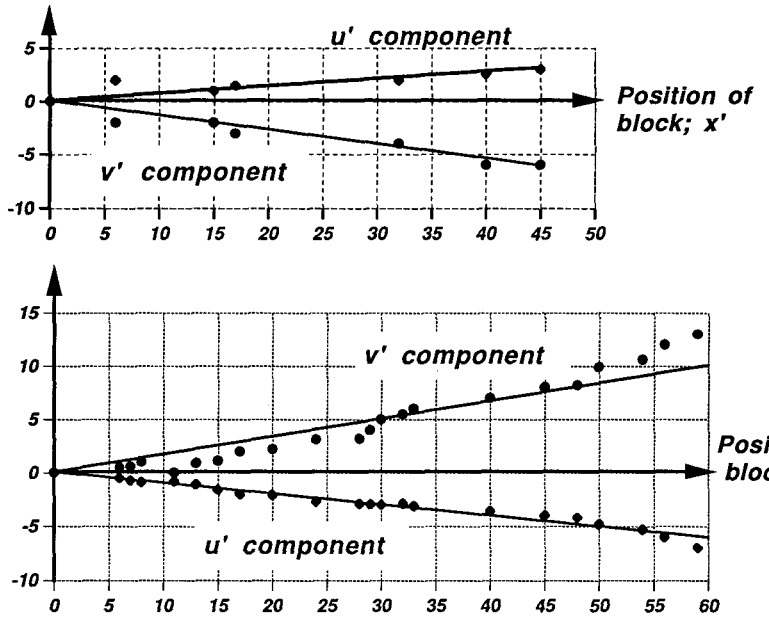

B.

Fig. A-2(B) Plots of measured reciprocal displacement components u' and v' against x' and against y'. The slopes of the plots give the values of the displacement gradients. In this example, $\Delta u'/\Delta x' = 0.07$, $\Delta v'/\Delta x' = -0.14$, $\Delta u'/\Delta y' = -0.10$, and $\Delta v'/\Delta y' = 0.17$.

where **i** and **j** are unit vectors parallel to the x' and y' coordinate axes, respectively. The location of each block in the deformed state is given by the coordinate values denoting the block's position along the traverse; (x'[C],0) denotes the position of block C in a traverse along the x' axis in fig. A-1, for example. After reading the reciprocal displacement of each block from the displacement diagram, we then plotted reciprocal displacement components u' and v' against position coordinates x' and y' (fig. A-2). The slopes of these four curves are the values of the reciprocal displacement gradients, $\Delta u'/\Delta x'$, $\Delta u'/\Delta y'$, $\Delta v'/\Delta x'$, and $\Delta v'/\Delta y'$ (fig. A-2B). Following Wojtal (1989), the displacement gradient values determine the magnitudes of the components of the reciprocal deformation matrix [**E**]. For the example given in fig. A-2,

$$[\mathbf{E}] = \begin{vmatrix} 1 + \Delta u'/\Delta x' & \Delta u'\Delta y' \\ \Delta v'/\Delta x' & 1 + \Delta v'\Delta y' \end{vmatrix} = \begin{vmatrix} 1.07 & -0.10 \\ -0.14 & 1.17 \end{vmatrix} \tag{A-2}$$

The reciprocal quadratic elonation matrix [λ'] is given by

$$[\lambda'] = [\mathbf{E}]^{\mathrm{T}}[\mathbf{E}] \tag{A3}$$

(see Wojtal, 1989). In this case

$$[\lambda'] = \begin{vmatrix} 1.15 & -0.27 \\ -0.27 & 1.39 \end{vmatrix}$$

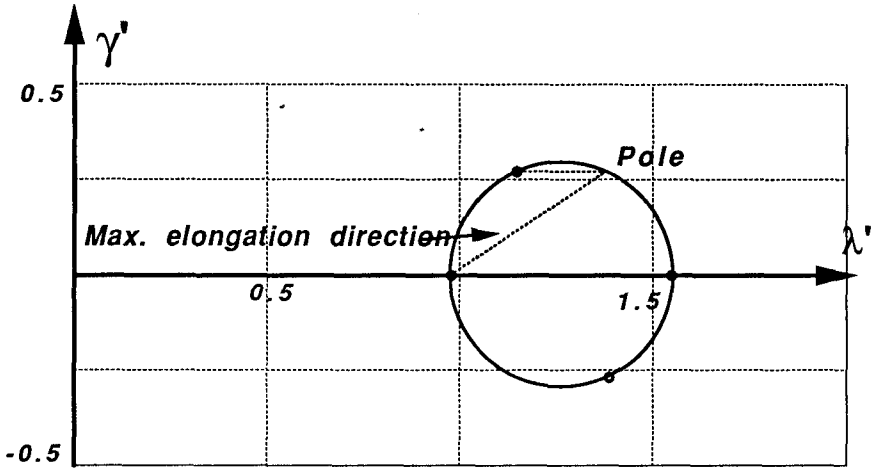

Fig. A-3. Reciprocal quadratic elongation Mohr diagram for sample 91110. Diagram indicates that $\lambda'_1 = 1.55$ and $\lambda'_2 = 0.98$. Pole to the Mohr diagram fixes the orientation of principal axes (see Wojtal, 1989 for additional information).

Finally, we construct a reciprocal quadratic elongation Mohr diagram for the sample and from that determine the magnitudes of the principal strains and their orientations relative to the arbitrary Cartesian coordinate axes. For sample 91110, for example, $\lambda'_1 = 1.55$ and $\lambda'_2 = 0.98$ (fig. A-3). The axial ratio of the corresponding strain ellipse is, then, $\sqrt{(\lambda'_1/\lambda'_2)} = 1.26$, and the area ratio of that strain ellipse is $[\sqrt{(\lambda'_1 \cdot \lambda'_2)}]^{-1} = 0.81$.

References

Alvarez, W., and Engelder, T., 1976, Formation of spaced cleavage and folds in brittle limestone by dissolution: Geology, v. 4, p. 698–701.

Alvarez, W., Engelder, T., and Geiser, P., 1978, Classification of solution cleavage in pelagic limestones: Geology, v. 6, p. 263–266.

Arthaud, F., 1969, Méthode de détermination graphique des directions de raccourassement, d'allongement et intermédiare d'une population des failles: Société Géologique de France, Bulletin, séries 7, v. 11, p. 729–737.

Arthaud, F., and Mattauer, M., 1969, Exemples de stylolites d'origine tectonique dans le Languedoc, leurs rélations avec la tectonique cassante: Société Géologique de France, Bulletin, séries 7, v. 11, p. 738–744.

Behzadi, H., and Dubey, A. K., 1980, Variation of interlayer slip in space and time during flexural folding: Journal of Structural Geology, v. 2, p. 453–457.

Bell, T. H., and Cuff, C., 1989, Dissolution, solution transfer, diffusion vs. fluid flow and volume loss during deformation/metamorphism: Journal of Metamorphic Geology, v. 7, p. 425–447.

Chapple, W. M., and Spang, J. H., 1974, Significance of layer-parallel slip during folding of layered sedimentary rocks: Geological Society of America Bulletin, v. 85, p. 1523–1534.

Currie, J. B., Patnode, H. W., and Trump, R. P., 1962, Development of folds in sedimentary strata: Geological Society of America Bulletin, v. 73, p. 655–674.

de Witt, W., Jr., and Colton, G. W., 1964, Bedrock geology of the Evitts Creek and Pattersons Creek quadrangles, Maryland, Pennsylvania, and West Virginia: U.S. Geological Survey Bulletin, v. 1173, p. 90.

Dean, S. L., Kulander, B. R., and Skinner, J. M., 1988, Structural chronology of the Alleghenian orogeny in Southeast West Virginia: Geological Society of America Bulletin, v. 100, p. 299–310.

Dubey, A. K., 1982, Development of interlayer slip in non-cylindrical flexural slip folds: Geoscience Journal, v. 3, p. 103–108.

Dubey, A. K., and Cobbold, P. R., 1976, Noncylindrical flexural slip folds in nature and experiment: Tectonophysics, v. 38, p. 223–239.
Dunne, W. M., 1988, Day Two—Valley and Ridge Province in Eastern West Virginia, *in* Woodward, N. B., editor, Geometry and Deformation Fabrics in the Central and Southern Appalachian Valley and Ridge and Blue Ridge: International Geological Congress, 28th, Washington, D.C., Field Trip Guidebook, T357, p. 15–24.
Durney, D. W., and Ramsay, J. G., 1973, Incremental strains measured by syntectonic crystal growths, *in* DeJong, K. A., and Scholten, R., editors, Gravity and Tectonics: New York: Wiley, p. 67–96.
Elliott, D., 1970, Determination of finite strain and initial shape from deformed elliptical objects: Geological Society of America Bulletin, v. 81, p. 2221–2236.
———— 1973, Diffusion flow laws in metamorphic rocks: Geological Society of America Bulletin, v. 84, p. 2645–2664.
Engelder, T., 1984, The role of pore water circulation during the deformation of foreland fold and thrust belts: Journal of Geophysical Research, v. 89, p. 4319–4325.
Engelder, T., and Geiser, P. A., 1979, The relationship between pencil cleavage and lateral shortening within the Devonian section of the Appalachian Plateau, New York: Geology, v. 7, p. 460–464.
Engelder, T., and Marshak, S., 1985, Disjunctive cleavage formed at shallow depths in sedimentary rock: Journal of Structural Geology, v. 7, p. 327–343.
Etheridge, M. A., Wall, V. J., Cox, S. F., and Vernon, R. H., 1984, High fluid pressures during regional metamorphism and deformation; implications for mass transport and deformation mechanisms: Journal of Geophysical Research, v. 89, p. 4344–4356.
Faill, R. T., 1973, Kink-band folding, Valley and Ridge Province, Pennsylvania: Geological Society of America Bulletin, v. 84, p. 1289–1314.
Fischer, M. P., Woodward, N. B., and Mitchell, M. M., 1992, The kinematics of break-thrust folds: Journal of Structural Geology, v. 14, p. 451–460.
Geiser, P. A., 1974, Cleavage in some sedimentary rocks of the central Valley and Ridge Province, Maryland: Geological Society of America Bulletin, v. 85, p. 1399–1412.
———— 1988a, Mechanisms of thrust propagation: some examples and implications for the analysis of overthrust terranes: Journal of Structural Geology, v. 10, p. 829–845.
———— 1988b, The role of kinematics in the construction and analysis of geologic cross sections in deformed terranes, *in* Mitra, G., and Wojtal, S., editors, Geometries and Mechanisms of Thrusting with Special Reference to the Appalachians: Geological Society of America Special Paper 222, p. 47–76.
Geiser, P. A. and Sansone, S., 1981, Joints, microfractures, and the formation of solution cleavage in limestone: Geology, v. 9, p. 280–285.
Gray, M. B., and Mitra, G., 1993, Migration of deformation fronts during progressive deformation: evidence from detailed structural studies in Pennsylvania Anthracite region, U.S.A.: Journal of Structural Geology, v. 15, p. 435–450.
Gwinn, V. E., 1964, Thin-skinned tectonics in the Plateau and Valley and Ridge Provinces of the central Appalachians: Geological Society of America Bulletin, v. 75, p. 863–900.
———— 1970, Kinematic patterns and estimates of lateral shortening, Valley and Ridge Provinces, central Appalachians, south central Pennsylvania, *in* Fisher, G. W., Pettijohn, F. J., Reed, J. C., and Weaver, K. N., editors, Studies of Appalachian geology, central and southern: New York, Wiley-Interscience, p. 127–146.
Helmstaedt, H., and Greggs, R. G., 1980, Stylolitic cleavage and cleavage refraction in lower Paleozoic carbonate rocks of the Great Valley, MD: Tectonophysics, v. 66, p. 99–114.
Henderson, J. R., Wright, T. O., and Henderson, M. N., 1986, A history of cleavage and folding: An example from the Goldenville Formation, Nova Scotia: Geological Society of America Bulletin, v. 97, p. 1354–1366.
Hudleston, P. J., 1986, Extracting information from folds in rocks: Journal of Geological Education, v. 34, p. 237–244.
Jamison, W. R., 1987, Geometric analysis of fold development in overthrust terranes: Journal of Structural Geology, v. 9, p. 207–219.
Kamb, W. B., 1959, Petrofabric observations from Blue Glacier, Washington, in relation to theory and experiment: Journal of Geophysical Research, v. 64, p. 1891–1909.
Kulander, B. R., and Dean, S. L., 1986, Structure and tectonics of the central and southern Appalachian Valley and Ridge and Plateau provinces, West Virginia and Virginia: American Association of Petroleum Geologists Bulletin, v. 70, p. 1674–1684.
Lewis, A. E., 1984, Biostatistics: New York, Van Nostrand Reinhold Co., p. 198.
Manz, R., and Wickham, J., 1978, Experimental analysis of folding in simple shear: Tectonophysics, v. 44, p. 79–90.

Marshak, S., and Engelder, T., 1985, Development of cleavage in limestones of a fold and thrust belt in Eastern New York: Journal of Structural Geology, v. 7, p. 345–359.
Means, W. D., 1987, A newly recognized type of slickenside striation: Journal of Structural Geology, v. 9, 585–590.
Meyer, T. J., and Dunne, W. M., 1990, Deformation of Helderberg limestones above the blind thrust system of the central Appalachians: Journal of Geology, v. 98, 108–117.
Mitra, S., 1978, Microscopic deformation mechanisms and flow laws in quartzites within the South Mountain Anticline: Journal of Geology, v. 6, 129–152.
———— 1986, Duplex structures and imbricate thrust systems: Geometry, structural position, and hydrocarbon potential: Geological Society of America Bulletin, v. 70, p. 1087–1112.
———— 1987, Regional variations in deformation mechanisms and structural styles in the central Appalachian orogenic belt: Geological Society of America Bulletin, v. 98, p. 569–590.
———— 1992, Balanced structural interpretations in fold and thrust belts, *in* Mitra, S., and Fisher, G. W., editors, Structural Geology of Fold and Thrust Belts: Baltimore, Maryland, Johns Hopkins University Press, p. 53–77.
Nickelsen, R. P., 1988, Structural evolution of folded thrusts and duplexes on a first-order anticlinorium in the Valley and Ridge Province of Pennsylvania, *in* Mitra, G., and Wojtal, S., editors, Geometries and Mechanisms of Thrusting with Special Reference to the Appalachians: Geological Society of America Special Paper 222, p. 89–106.
Perry, W. J., 1978, Sequential deformation in the Central Appalachians: American Journal of Science, v. 278, p. 518–542.
Perry, W. J., Jr., and de Witt, W., Jr., 1977, A field guide to thin skinned tectonics in the central Appalachians: American Association of Petroleum Geologists, National Meeting Guidebook, p. 1–54.
Price, N. J., and Cosgrove, J. W., 1990, Analysis of Geological Structures: Cambridge: Cambridge University Press, 502 p.
Price, R. A., 1967, The tectonic significance of mesoscopic subfabrics in the southern Rocky Mountains of Alberta and British Columbia: Canadian Journal of Earth Sciences, v. 4, p. 39–70.
Ramsay, J. G., 1967, Folding and fracturing of rocks: New York, McGraw-Hill Book Company, 568 p.
———— 1974, Development of chevron folds: Geological Society of America Bulletin, v. 85, p. 1741–1754.
———— 1976, Displacement and strain: Philosophical Transactions of the Royal Society of London, v. A273, pp. 3–25.
———— 1980, Shear zone geometry: A review: Journal of Structural Geology, v. 2, 83–99.
Ramsay, J. G., and Huber, M. I., 1987, The Techniques of Modern Structural Geology. Volume II: Folds and Fractures: London, Academic Press, p. 309–700.
Rutter, E. H., 1976, The kinematics of rock deformation by pressure solution: Philosophical Transactions of the Royal Society of London, v. A283, p. 203–220.
Schmid, S. M., Boland, J. N., and Paterson, M. S., 1977, Superplastic flow in fine-grained limestone: Tectonophysics, v. 43, p. 257–292.
Schumaker, R. C., Wilson, T. H., Dunne, W. M., Knotts, J., and Buckey, R., 1985, Pennsylvania, Virgin, and West Virginia Sections, *in* Woodward, N. B., editor, Valley and Ridge Thrust Belt: Balanced Structural Sections, Pennsylvania to Alabama: University of Tennessee Department of Geological Sciences Studies in Geology, v. 12, p. 6–36.
Smith, R. B., 1979, The folding of a strongly non-Newtonian layer. American Journal of Science, v. 279, p. 272–287.
Srivastava, D. C., and Engelder, T., 1990, Crack-propagation sequence and pore-fluid conditions during fault-bend folding in the Appalachian Valley and Ridge, central Pennsylvania: Geological Society of America Bulletin, v. 102, 116–128.
Suppe, J., 1983, Geometry and kinematics of fault-bend folding: American Journal of Science, v. 283, 684–721.
———— 1985, Introduction to Structural Geology: Englewood Cliffs, New Jersey, Prentice Hall, Inc., 537 p.
Tanner, P. W. G., 1989, The flexural-slip mechanism: Journal of Structural Geology, v. 11, 635–655.
———— 1992, The duplex model: Implications from a study of flexural-slip duplexes, *in* McClay, K. R., editor, Thrust Tectonics: London, Chapman & Hall, p. 201–208.
Weyl, P. K., 1959, Pressure solution and force of crystallization—a phenomenological theory: Journal of Geophysical Research, v. 64, p. 2001–2025.

Willis, B., 1893, Mechanics of Appalachian structure: U.S. Geological Survey Annual Report 13 (1891–1982), part 2, p. 217–281.

Wilson, T. H., and Schumaker, R. C., 1992. Broad Top thrust sheet: An extensive blind thrust in the central Appalachians: American Association of Petroleum Geologists Bulletin, v. 76, p. 1310–1324.

Wojtal, S., 1989, Measuring displacement gradients and strains in faulted rocks: Journal of Structural Geology, v. 11, p. 669–678.

Woodward, N. B., 1992, Deformation styles and geometric evolution of some Idaho-Wyoming thrust belt structures, *in* Mitra, S., and Fisher, G. W., editors, Structural Geology of Fold and Thrust Belts: Baltimore, Maryland, Johns Hopkins University Press, p. 191–206.